UNIVERSIDAD AUTÓNOMA DE MADRID

ESCUELA POLITÉCNICA SUPERIOR

Grado en Ingeniería de Tecnologías y Servicios de Telecomunicación

TRABAJO FIN DE GRADO

ANTENA COMPACTA DE DOBLE LAZO PARA OPERACIÓN MULTIBANDA EN DISPOSITIVOS CON SENSORES

Autora: Esther Álvarez Pardo

Tutor: Jordi Romeu Robert

Ponente: José Luis Masa Campos

Julio 2017

COMPACT DUAL-LOOP ANTENNA FOR MULTIBAND OPERATION IN SENSOR DEVICES

AUTHOR: Esther Álvarez Pardo

ADVISOR: Jordi Romeu Robert (*)

CO-ADVISOR: José Luis Masa Campos (**)

(*) Escuela Técnica Superior de Ingeniería de Telecomunicación de Barcelona

Universitat Politècnica de Catalunya

(**) Escuela Politécnica Superior

Universidad Autónoma de Madrid

Julio 2017

Dedicated to Fernando, Mari Luz and Mario.

Thank you for the endless support.

Title of the thesis: Compact dual-loop antenna for multiband operation in sensor devices.

Author: Esther Álvarez Pardo.

Advisor: Jordi Romeu Robert.

Co-advisor: José Luis Masa Campos.

Abstract

The aim of this Bachelor Thesis is to design, simulate and optimize a compact dual-loop antenna in order to have resonant frequencies in the bands 800-1000 MHz and 1700-1900 MHz, suitable to be integrated within sensors.

Due to the rising number of smart interconnected devices that operate at different frequency bands, constituting what is known as the Internet of Things, it is necessary to provide with an antenna that not only enables communication - regardless the location -in an efficient way, but also that is cost-effective, easy to produce and durable.

For this purpose, a first design was implemented, following the article [1] "Folded Dual-Loop Antenna for GSM/DCS/PCS/UMTS Mobile Handset Applications". To analyse its behaviour throughout the simulations, the software tool CST Microwave Studio (Computer Simulation Technology) was employed.

During this project, several optimizations were realized along with the design process so as to have the antenna working for the two main frequency bands employed by the wireless systems: Global System for Mobile Communications (GSM: 890–960 MHz) and, Digital Cellular System (DCS: 1710–1880 MHz); taking into account as well the casing effects of the sensor device.

Once the performance of the proposed design complied with the requirements with 10 dB return loss, the antenna was fabricated. In order to validate the previous simulation results' accuracy, the antenna was measured with and without its resin casing, physically representing the same design that was developed at CST Microwave Studio.

Finally, the presented design proved to achieve good results and fractional bandwidth at a lower cost when compared to existing solutions for internal antennas within sensor devices.

Título del Trabajo de Fin de Grado: Compact dual-loop antenna for multiband operation in sensor devices.

Autora: Esther Álvarez Pardo.

Tutor: Jordi Romeu Robert.

Ponente: José Luis Masa Campos.

Resumen

El objetivo de este Trabajo de Fin de Grado es diseñar, simular, y optimizar una antena compacta de doble lazo para obtener frecuencias de resonancia en las bandas 800-1000 MHz y 1700-1900 MHz, apta para ser integrada con sensores.

Debido al creciente número de dispositivos inteligentes interconectados que operan en diferentes bandas de frecuencia, constituyendo lo que se conoce como el Internet de las Cosas, es necesario producir una antena que no sólo habilite la comunicación - independientemente de la localización - de una manera eficiente, sino que también sea rentable, fácil de producir y duradera.

Para este propósito, se implementó un primer diseño, siguiendo el artículo [1] "Folded Dual-Loop Antenna for GSM/DCS/PCS/UMTS Mobile Handset Applications". Para analizar su comportamiento a través de las simulaciones, se utilizó la herramienta de software CST Microwave Studio (Tecnología de Simulación Computacional).

Durante este proyecto, varias optimizaciones se llevaron a cabo junto con el proceso de diseño para tener una antena funcionando en las dos bandas principales de frecuencia utilizadas por los sistemas inalámbricos: Sistema Global de Comunicaciones Móviles (GSM: 890–960 MHz) y, Sistema Celular Digital (DCS: 1710–1880 MHz); teniendo también en cuenta los efectos de la carcasa del sensor.

Una vez que el comportamiento del diseño propuesto cumplía con los requisitos para pérdidas de retorno a 10 dB, la antena fue fabricada. Para validar la exactitud de los resultados de simulación previos, la antena se midió no sólo con su carcasa de resina sino también sin ella, representando físicamente el mismo diseño desarrollado en CST Microwave Studio.

Finalmente, el diseño presentado demostró conseguir buenos resultados y ancho de banda fraccional a un coste más bajo al compararse con soluciones existentes para antenas internas en dispositivos con sensores.

Acknowledgements

I would like to express my gratitude to Prof. Jordi Romeu for giving me the opportunity to develop this project. There are no words to describe how privileged I feel for having your support and guidance throughout this year.

Thanks to Prof. José Luis Masa Campos and Marc Imbert for their advice and feedback, and the laboratory technicians Ruben Tardio and Albert Marton for their support and fabrication of the antenna.

I would also like to thank my lifetime friend Judit for believing in me during all these years, encouraging me to keep moving forward.

Special thanks to my parents Mari Luz and Fernando, and my brother Mario for being an inspiration and standing by my side in the tough times of my career and life. I wouldn´t be who I am now without you.

And last but not least, I would like to thank that one person who did not give up on me and was always there.

Keywords

Internet of things, IoT, dual-loop, compact, antenna, multiband, mobile, handset, device, CST, GSM, DCS, PCS, UMTS, sensor, embedded, integrated, fractional bandwidth, FBW, low cost, low profile, small size, PIFA, internal antenna, PCB, light weight, easy fabrication, casing, VNA, coaxial, SMA, TEM, strip, FR4.

Palabras clave

Internet de las cosas, IoT, doble lazo, compacta, antena, multibanda, móvil, dispositivo, CST, GSM, DCS, PCS, UMTS, sensor, embebido, integrado, ancho de banda fraccional, FBW, bajo coste, perfil bajo, pequeño tamaño, PIFA, antena interna, PCB, peso ligero, fácil fabricación, carcasa, VNA, coaxial, SMA, TEM, strip, tira, FR4.

Table of contents

List of Figures

List of Tables

1. Introduction

1.1. Introduction to the Internet of Things (IoT)

Nowadays, our everyday life is surrounded by wireless devices and artefacts that can be connected with an on and off switch to the Internet. These systems of interconnected devices, which are embedded with electronics, sensors, actuators and software to exchange and collect data, are what is called The Internet of Things (IoT). Therefore, every common object such as the appliances at home, clothes and furniture among others, can communicate the information required becoming both more "intelligent" and independent.

In the field of electromagnetism, to develop small size antennas to be integrated within sensor devices is key to realize the data transmission while being able to place the device anywhere, providing a faster, smoother and cheaper flow of information.

For this reason, a limiting factor in modern electronics is that large antennas are not compatible with electronic circuits, which are shrinking everyday.

Other obstacles associated with the IoT include providing reliable connectivity and maintaining reasonably performance with a compact antenna size, despite being sited in the most challenging environments for radio propagation.

To this end, antenna design with some desirable features such as multiband operation, low profile, light weight, and easy fabrication have earned high attention for practical applications.

1.2. Requirements and specifications

The network topology of IoT systems is composed of simple nodes or devices which sense, gather and transmit a certain amount of information to a gateway or central controller that provides the Internet and cloud services connectivity.

Communication between nodes and a centralized "cloud" must be secure in order to protect and process the data stored, enabling the sensor devices to bounce actionable information down to humans. Moreover, these nodes and gateways must be designed in order to keep the power consumption at its minimum as well as providing a large wireless connectivity range.

Thus, in order to deploy networks of IoT devices, both the network and the antenna must be specified, which means that the type of wireless network to be used for connectivity should be determined, and consequently, the antenna (or multiple antennas) needed to comply with the device´s design and physical properties. For instance, 900MHz, 2.4GHz and 5GHz radios may all have different requirements for the antenna design.

The following subsection focuses on this last part, covering IoT antennas of various types that will help IoT module designers to make the right choice of antenna, which is of interest for the purpose of this project.

1.2.1. Antenna types for the IoT

IoT devices are usually very small and ubiquitous, for this reason, compact size, low-power consumption and high reliability are the three main factors to take into account in the antenna design.

If the physical space is a priority, the design to implement is commonly the prefabricated chip antennas, which is relatively easy to realize and cost effective when produced in high volumes. Chip antennas (see Figure 1.1) are surface-mount devices used for frequencies that range from 300 MHz to 2500 MHz with a size that goes from 2 up to 20 square millimetres in length, becoming the smallest design available.

They are manufactured on ceramic substrate or a small multi-layer Printed Circuit Board (PCB), which acts as the antenna ground and occupies half of the antenna system, the chip itself constitutes the other half.

However, chip antennas have a very narrow bandwidth, are strongly dependent on the ground plane, and must be made to the exact frequency.

Figure 1.1. Embedded ceramic multi-band chip antenna (taken from Pulse Electronics News).

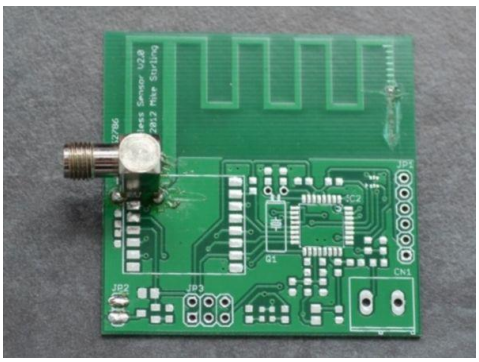

Figure 1.2. PCB antenna with test port attached (taken from Mike´s Lab Notes).

If the IoT devices contain multiple sensors and are meant for large-scale manufacturing, reduced unit cost and reasonable design flexibility will be considered significant matters.

In these cases, PCB antennas are regarded as the best option, with advantages that stem from the PCB´s highly refined manufacturing process.

PCB antennas (see Figure 1.2) perform well above 800 MHz and have a small size at high frequencies; performance challenges appear below 500 MHz, the size increases as the frequency decreases. It must be borne in mind that multiple antennas increase the PCB size and, redesigning the antenna requires redesigning the board as well.

PCB antennas can have a meandered conductor design, which means having a trace in a certain pattern on the circuit board, or they can be planar monopole. The typical types of printed antennas include patch antennas, inverted-F antennas (IFA), or planar inverted-F antennas (PIFA) (see Figure 1.3). Among their benefits it can be seen that the space taken by a PCB is less than by a dipole antenna (see Figure 1.4) due to using the ground plane of the circuit board to help them radiate. Variants include flexible printed circuit (FPC) and stamped metal antennas.

Figure 1.3. PIFA antenna (taken from Richard Langley thesis on PIFA antenna).

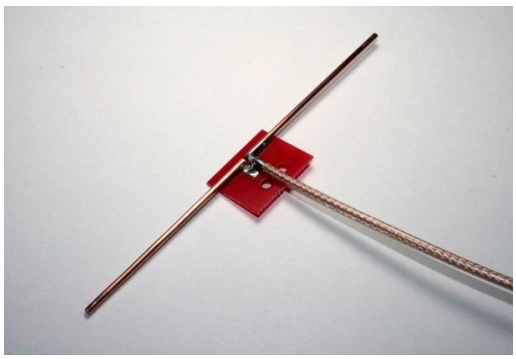

Figure 1.4. Fine-tuned dipole antenna (taken from Flytron).

The following option in terms of performance would be to source a proprietary antenna, which is custom-designed in order to meet the desired specifications. In this case, it´s critical to know the exact use case for the antenna to completely describe and design the performance dynamics, enabling the antenna to be designed for maximum efficiency. One of the main drawbacks of choosing proprietary antenna designs is the cost, which can be reduced if using a pre-tuned standard antenna that can be integrated onto a PCB assembly while ensuring high quality.

In those cases where the budget is tight, a fair option is the wire antenna (see Figure 1.5). Wire antennas increase in size by a decrement in frequency and require more testing and simulation regarding electromagnetic performance. However, several wire antennas can be attached to a module board via micro-coaxial cable, which makes them suitable when multiple wireless technology transceivers are needed for the IoT device. Also, the prototype design is very cost effective and allows for several tested versions during its development.

Nevertheless, a tradeoff between maximum performance and price can be found in the whip antennas (see Figure 1.6). Even though they are external and require a connector to the PCB module, interferences when dealing with multiple transceivers can be avoided.

Figure 1.5. A wire antenna kit with a coil of wire, strain insulators and a balun (taken from Wikipedia).

Figure 1.6. Sennheiser A182 whip antenna for Evolution Series (Frequency B).

Finally, it must be noticed that higher frequency systems are preferred in terms of space limitations since the higher the frequency, the lower the wavelength and thus, a more compact antenna design is doable at a cost of reducing the distance that lower frequencies achieve for communication. In practice, many IoT applications prefer the 868 MHz band in Europe and the 915 MHz band in the USA; in these bands the propagation is more reliable and the wavelength is larger than 30 cm (at the speed of light c, the wavelength is given by $\lambda=c/f$).

Furthermore, when selecting between an external antenna, or embedding one into the module itself, designers must consider the material and the potential placement of the product regarding how difficult it is to get a wireless signal from the nearest gateway.

1.3. Motivation and statement of purpose

As “International Journal of Antennas and Propagation” explains in [2], according to analysts, the Internet of Things´ number of connected devices is increasing impressively, rising the figure of 50 billion devices and enabling the emergence of new smart objects that operate at different frequency bands, bandwidths and power levels.

With this technology boom comes the need to provide the wireless communication systems with reliable data transmission, which requires advanced investigation in the field

of antenna design. Therefore, the electromagnetic properties of the environment, where the smart devices that gather the data are placed, must be taken into account during the antenna modelling.

In this aspect is where the thesis focuses, realizing a PIFA antenna design and optimization in an IoT framework, finding a compromise between performance and size while minding the fabrication price. The goal is to achieve the same performance as existing solutions while reducing the cost and size significantly.

The already marketed solution to compare with, consists of a PCB module with an external pentaband antenna that covers the frequency bands:

- 824.4 to 960 MHz
- 1710 to 2170 MHz.

Where the PCB module is 60(L) x 70(W) mm^2 and it´s located inside a casing with the following measures (see Figure 1.7):

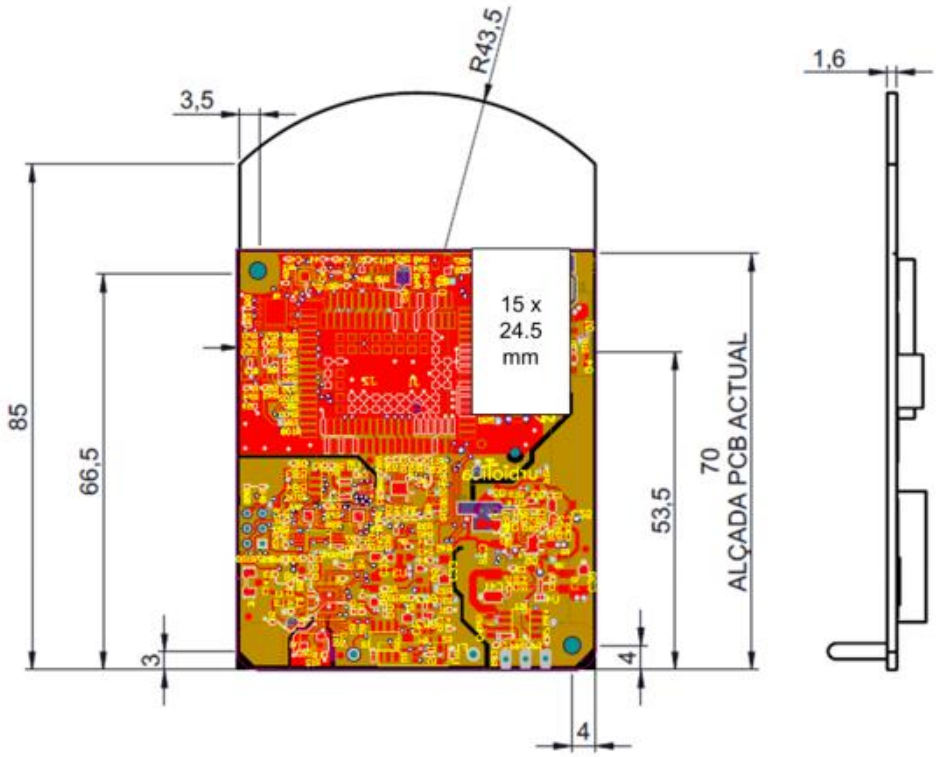

Figure 1.7. Existing solution´s PCB module and its casing.

In this project, the proposed PIFA antenna covers the same frequency bands by means of a dual-loop design with a compact size, which is compatible with the existing sensor device. In addition, it is embedded in the casing along with the PCB module, complying in this way with the IoT requisites.

The purpose of the proposed system, as well as of the existing system, is to gather and process through the sensor device the data collected of a garbage container in order to know whether it has reached its maximum level among other information. This is very useful when it comes to deploy a whole network of these sensors, actively storing and transmitting information in real time, which can be used to take action in a certain area or have a dynamic route for the dustmen while working, prioritizing the places where there is more waste accumulated. Moreover, this functionality helps to communicate whether any of the containers is having any kind of trouble such as cathing on fire, scrolling down or being placed upside down by anyone.

Last but not least, this antenna design can be used in any sensor that requires an antenna to communicate its data in an efficient way at an affordable price, having the properties of scalability to a network of sensor devices and a compact size to fit almost anywhere within its embedded system.

1.4. Project scope

The scope of this project is to simulate and optimize an alternative antenna design to be embedded within a sensor device in a resin casing in order to realize the same functions as an existing external antenna but at less cost and size, without compromising a good performance. The objectives to be achieved are:

- Design an efficient alternative IoT antenna to be integrated within sensors.

- Optimize the design in order to achieve the frequency bands' requirements with 10 dB return loss during the simulations.

- Repeat the process taking into account the casing effects of the device and how it affects the system's electromagnetic behaviour.

- Get the antenna fabricated in order to take real measurements of its performance and compare the results with the simulations.

- Redo the measurements with the antenna inside the resin casing and compare to both the simulations and the existing solutions (actual example taken, from "Company 1", and its competitor's solution, from "Company 2").

- Analyse all the results and present the conclusions. See whether they meet our original expectations.

1.5. Thesis organisation

This document is organized in chapters with the following content:

• Chapter 1: Starts with an introduction to the Internet of Things (IoT), followed by the requirements and specifications for each antenna type in the IoT framework, motivation and statement of purpose, project scope and thesis organisation.

• Chapter 2: with the objective to review what has previously been done in this research field, a state of the art of the technology used or applied in this thesis is presented.

• Chapter 3 explains in detail the methodology and project development carried out during the process of fulfilling the goals mentioned in the project scope, highlighting the initial steps that every design must take: antenna modelling, structure and ports among others. An optimization process coexists with the design stage.

• Chapter 4: the fabrication process and specifications for the antenna are commented. Also, the implementation changes made from the final simulated design, and the environmental impact.

• Chapter 5 addresses the analysis of the results obtained by measuring the available antennas and its comparison with the results that appeared in the simulation.

• Chapter 6: last conclusions are drawn to summarize the project results and contributions. Future steps related to the project are underlined as well as its practical applications.

• Chapter 7 is constituted by the appendix, which includes all the radiation diagrams from section 5.2.

2. State of the art

The growth in the antenna design field has exploded with the rapid evolution of communication technologies. Many studies have been carried out within this aspect such as [4] where a built-in folded monopole antenna is modified and analysed so as to get a small size, good performance and low profile by folding a loop element sideways.

Moving on to [5], a compact antenna size is achieved for mobile handsets using a feeding strip, shorting strip and a folded loop radiating element with embedded tuning notches. Same goal is addressed by [6]-[8] employing an internal antenna with a bent-shaped structure for multiband operation implementation in handset devices.

With regards to [9], a broadband internal antenna formed by a combination of a shorted monopole and a loop type antenna is proposed. Despite being small and having a simple structure, it performs with wide impedance bandwidths, high antenna gains and good radiation patterns. A FR4 substrate is used with 1mm thickness and 4.4 relative permittivity.

In addition, another research has been carried out in [10], where a hybrid loop/monopole slot antenna for quad-band operation in mobile phone devices is proposed. It is composed by a monopole slot antenna and a meandered loop antenna operating at GSM/DCS/ PCS/UMTS systems, covered by two wide bands centred at 900 and 1900 MHz.

However, the above mentioned designs cannot be easily embedded inside a sensor device because of their large size. For this reason, our proposed antenna is mainly based on [1], using its results as a first approach to a better final design that really meets our specifications.

In [1], a compact folded dual-loop antenna for mobile handset applications is designed using a bent-shaped radiator, which consists of a pair of symmetric meander strips of small size (50(L) x 9(W) x 9(H) mm^3). This antenna design can be tuned by modifying the spaces g1 and g2 between the loops, achieving with its compact size the desired frequency bands covering 847–971 and 1670–2230 MHz. Thus, becoming a good option for integration within mobile handsets as an internal antenna.

Our project contribution to the state of the art in this field is to develop and modify the approach taken in [1] for mobile devices to provide with an internal antenna that can be embedded in sensor devices such as the one taken as an example from “Company 1”. Not only a compact and simple structure is achieved but also it is more cost-efficient than the existing solutions as it will be seen in the following sections. The wider impedance bandwidth obtained in comparison with the already marketed antennas is a huge benefit to consider as well.

3. Methodology / project development

3.1. Antenna design

3.1.1. Baseline design

In [1], the geometry of the presented folded dual-loop antenna (see Figure 3.1), consisting of a pair of symmetric meander strips, is designed with 1 mm union width using 0.2-mm-thick copperplate. The two loops that form the radiator are then bent, resulting in two perpendicular layers so as to achieve a compact size. As a consequence, the antenna final dimensions are just: 50(L) x 9(W) x 9(H) mm^3.

Regarding the ground plane, the same copperplate from the antenna is used with a size of 90(L) x 50(W) mm^2, which simulates the ground plane for general handset devices. In order to hold a mobile casing, a vertical shielding plane is used and connected to the ground plane (see Figure 3.2).

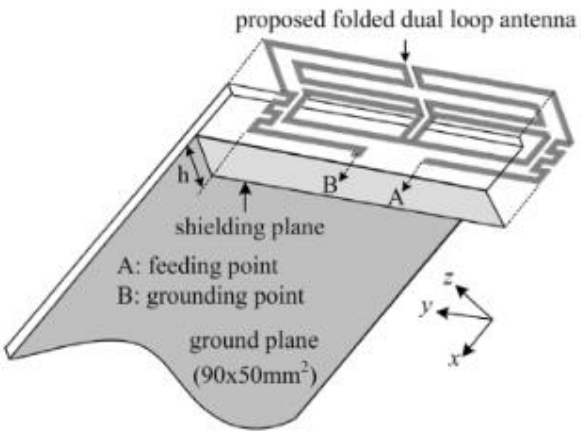

Figure 3.1. Folded dual-loop antenna design (taken from [1]).

Figure 3.2. Fabricated dual-loop antenna (taken from [1]).

For multiband operation, the longer loop (path A–C–D–E–F–G–H–I–B), (see Figure 3.3), works for the lower band and corresponds to one wavelength at 900 MHz. Working for the upper band, the shorter loop (path A–C–D–F–H–I–B) corresponds to one wavelength at 1800 MHz.

Furthermore, two gaps g1=1 mm, and g2=8 mm are designed to obtain good radiation and enable operating frequency tuning respectively.

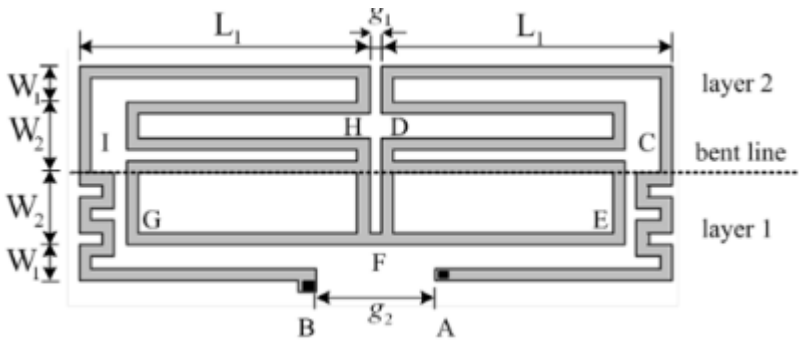

Figure 3.3. Optimized geometry design parameters of the presented dual-loop antenna (taken from [1]): L1=24.5 mm, W1=3 mm, W2=6 mm, g1=1 mm, g2=8 mm, h=8.8 mm.

The fabricated prototype for the baseline design (see Figure 3.2) was measured and tested, resulting in two impedance bandwidths with 6 dB return loss that satisfy the GSM/DCS/PCS/UMTS bands' requirements around 847–971 and 1670–2230 MHz (see Figure 3.4).

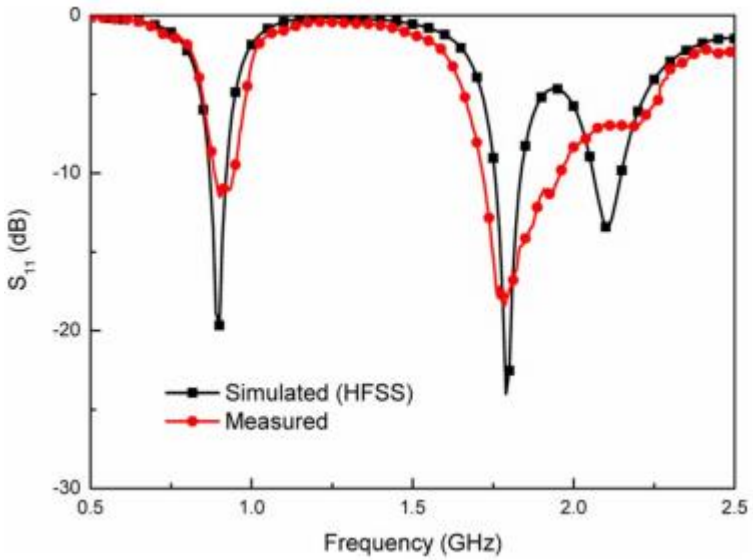

Figure 3.4. Simulated and measured return losses of the presented antenna (taken from [1]).

3.1.2. First approach

Taking into account the purpose and advantages of [1], a first design is realised to obtain the first simulation results that will lead to changes and advances to get closer to meet our desired specifications. A specialist tool for 3D electromagnetic simulation of high frequency components, CST Microwave Studio, has been used for an accurate analysis of the proposed antenna.

Thus, the first approach taken in the design (see Figures 3.5 and 3.6) has the same size and parameters as in [1], but instead of realizing a bent-shaped structure, it has been left plain flat on a FR4 substrate with 2(W) mm more than the surface dimensions from Figure 3.1 50(L) x 70(W) mm^2, plus the antenna dimensions 50(L) x 18(W) mm^2. The substrate, which is placed in between the antenna and the copper ground plane, has therefore the total dimensions of 50(L) x 90(W) mm^2. The copper ground plane constitutes the bottom layer in our design and its measures are the same as in Figure 3.1 plus 2(W) mm, which is, in total, 50(L) x 72(W) mm^2 (see Figures 3.7 and 3.8).

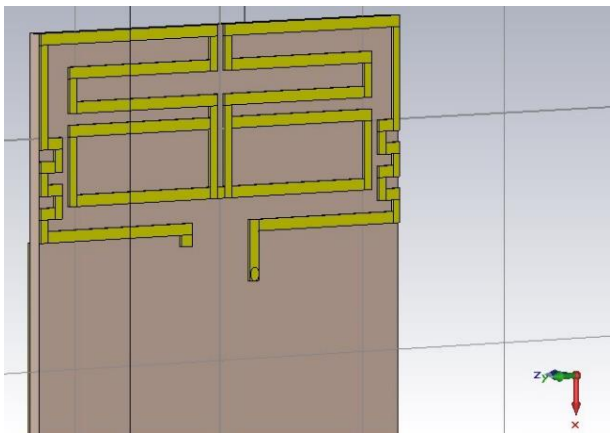

Figure 3.5. First approach front part of the dual-loop antenna design.

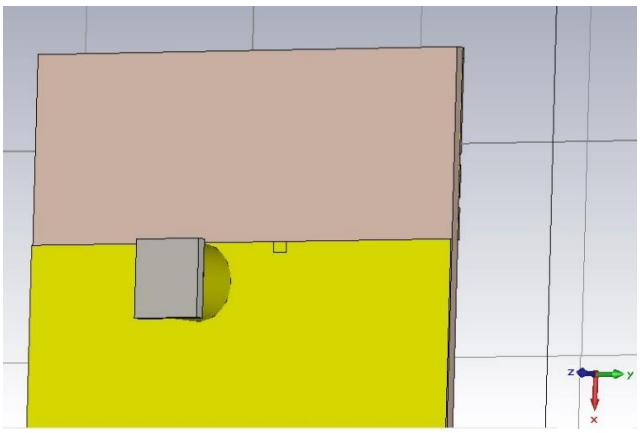

Figure 3.6. First approach back part of the dual-loop antenna design.

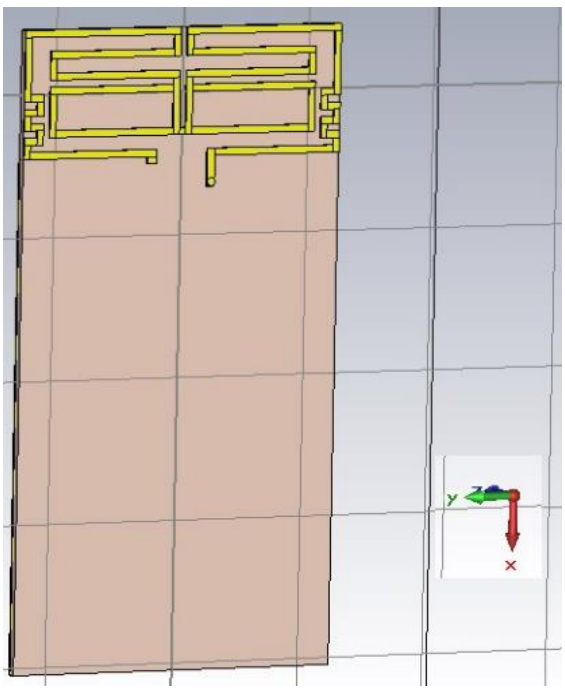

Figure 3.7. First approach complete front part of the dual-loop antenna design.

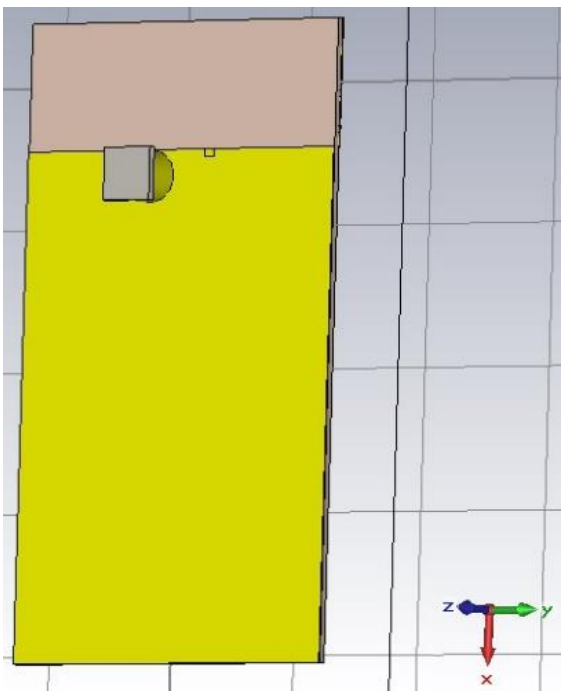

Figure 3.8. First approach complete back part of the dual-loop antenna design.

As you can see from the above pictures, our choice for the IoT antenna realization to be embedded in a PCB module with its casing, which is designed at the end of this chapter, is a PIFA antenna type. Our PIFA antenna contains the baseline design's meander strips in order to achieve the desired small size, at the cost of slightly reducing the fractional bandwidth.

However, unlike in the design made at [1], a balun to be connected between the feeding cable and the antenna won´t be used in the construction and testing of the proposed antenna. Instead, just a coaxial cable is employed and connected to the antenna feeding point A (see Figure 3.9). It should be noticed as well that the strip corresponding to the feeding point A is enlarged and connected to the ground copper plane through the selected substrate (FR4) via the chosen coaxial cable.

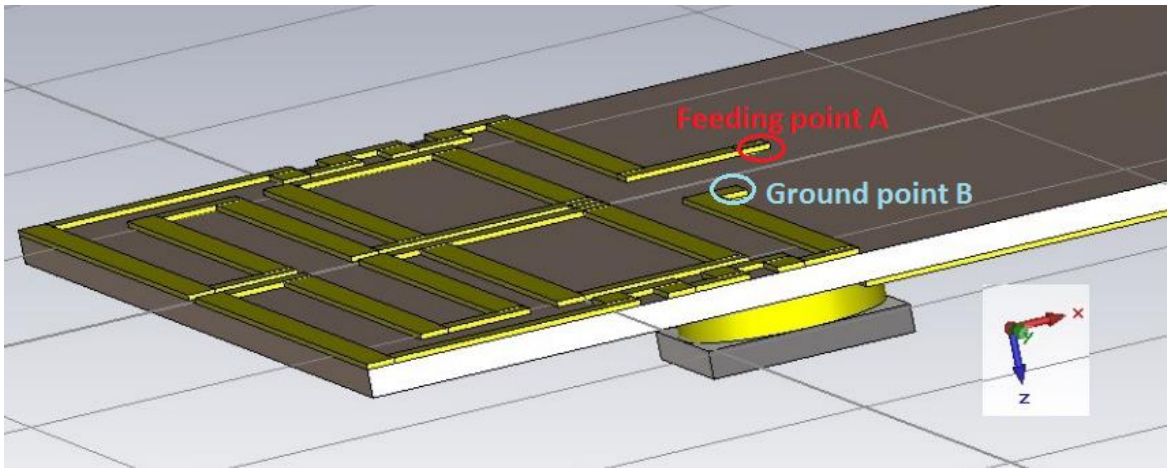

Figure 3.9. Antenna´s feeding point A and ground point B.

When performing the design, it should be taken into account that one of the most powerful characteristics of CST it that the 3D models are parametric. This is particularly useful when optimizing the antenna since it is enough to change the value of these parameters to change the dimensions of the antenna model, without redoing or manually adjusting the whole design.

As mentioned before, a coaxial (feeding structure) composed of an inner conductor, a dielectric and an outer conductor was included in CST to excite our antenna. Each one of the elements was created using the cylinder creation mode. The parameters needed to specify the radius of the cylinders and their length were the following:

CoaxL	= 5
Coax_r	= 0.6
CoaxR	= 2.01
CoaxR3	= 3.71

Figure 3.10. Coaxial cable's 50 Ω impedance parameters.

In Figure 3.10, CoaxL is the coaxial's length, from 0 to Coax_r is the inner conductor, from Coax_r to CoaxR is the dielectric and, from CoaxR to CoaxR3 is the outer conductor. The dimensions for the coaxial's structure (Coax_r, CoaxR and CoaxR3) were obtained in order to get a 50 Ω impedance matching following the next formula:

$$Z_0 = \frac{138}{\sqrt{\varepsilon_R}} \log\left(\frac{D}{d}\right) (ohms)$$

Where Er (relative permittivity) has the value of 2.1 for the Teflon material of the coaxial´s dielectric. Also, Coax_r is equal to half the value of d, CoaxR is equal to half the value of D and, D/d= 4.02/1.2= 3.35, which is one of the combinations that verify a characteristic impedance Zo= 50 Ω for the respective Er and, its measures are approximated to the size of some marketed connectors.

Furthermore, these values can be checked with an online coaxial impedance calculator such as the one in [11] (see Figure 3.11).

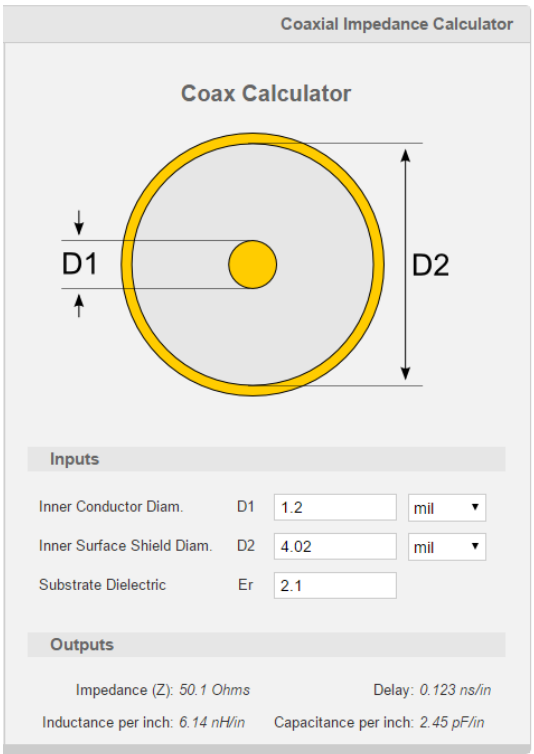

Figure 3.11. Coaxial parameters checked with an online calculator for Zo= 50 Ω.

Being D1= d= 2*Coax_r= 1.2 mm; and D2= D= 2*CoaxR= 4.02 mm.

Once the proper first approach design has been achieved, its electrical characteristics and radiation performance are analysed by obtaining the simulation of the antenna´s reflection parameter (S11) in dB as appears in the next screenshot (see Figure

3.12):

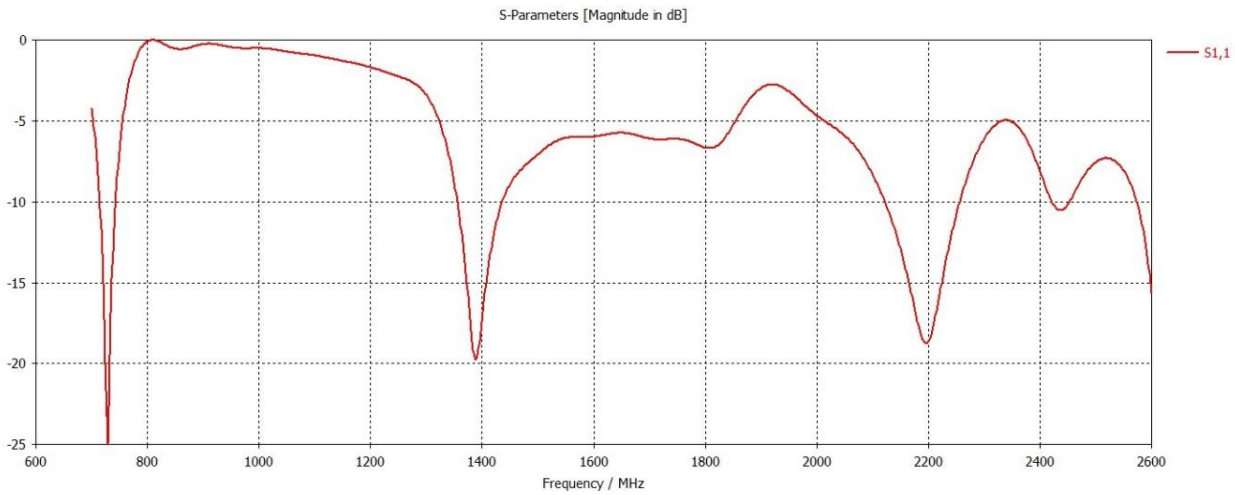

Figure 3.12. Antenna´s S11 parameter in dB.

It can be observed that there are three main resonant frequencies at around 750 MHz, 1400 MHz and 2200 MHz, which is not what we wanted but a good first simulation result in order to optimize and get the desired outcomes. It is expected to be different from the baseline designed simulation (see Figure 3.4) due to the changes applied and deviations regarding the material properties and the substrate layer.

Note: in CST the coaxial port should be declared, this means it is necessary to add the excitation port to the antenna device, for which the reflection parameter is later calculated. The port simulates an infinitely long coaxial waveguide structure that is connected to the structure at the ports plane (see the definition process in Figures 3.13 and 3.14).

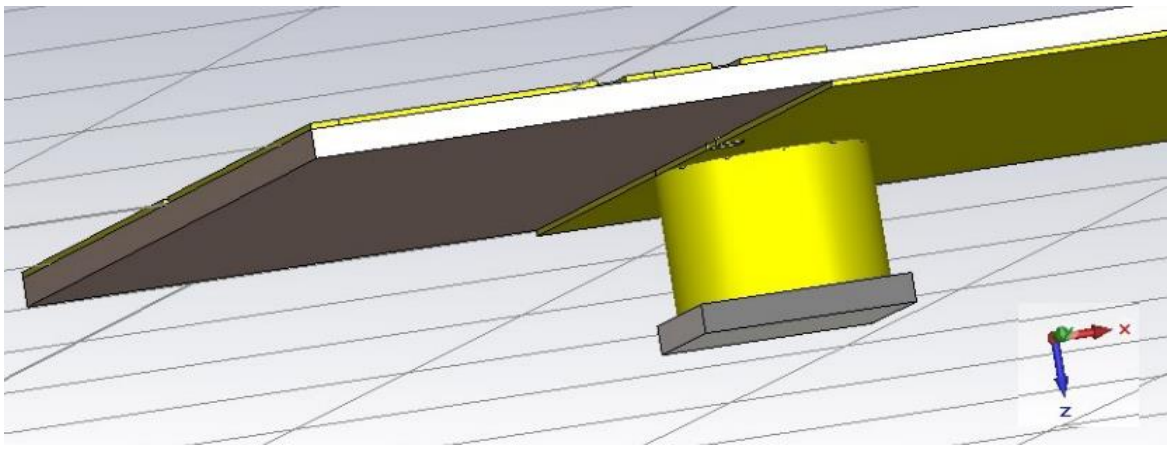

Figure 3.13. Antenna´s 50 Ω coaxial structure.

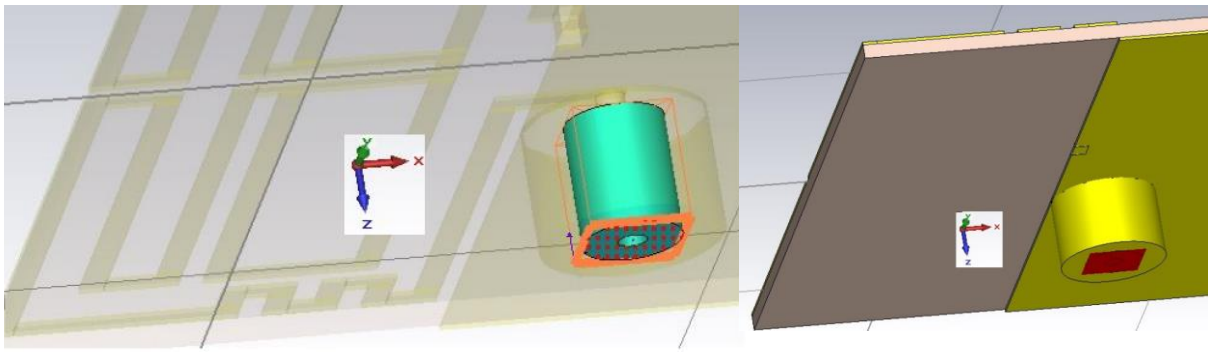

Figure 3.14. Waveguide port definition.

3.1.3. First optimization

The antenna optimization consists of a first stage of trial and error where we detect how the different parameters influence the antenna's behaviour. As a first practical method, it can be proven that, in order to position a resonant frequency in a different operational frequency, the following rule applies:

The new chosen antenna length is the antenna´s current length times the current resonant frequency over the desired resonant frequency.

*New_L= Current_L*Current_freq/ Desired_freq*

With this rule, the length that the antenna must have in order to achieve the expected resonant frequency can be calculated given the non-desired current values of the antenna's length and operational frequency.

Moreover, changing the value of g1 implies a change in the low frequency levels (reducing the g1 value, places the antenna's low-band operational point even lower in frequency) and, incrementing carefully the g2 value contributes to a better performance in the high frequencies due to a reduction of the ripples that appear in the Figure 3.12 S11 parameter's graphic.

Thus, for the first set of final values (see Figure 3.15):

- Antenna Total Length= 34 mm.
- Antenna Total Width= 18 mm (same value as before).
- g1= 1.5 mm.
- g2= 11 mm.

The following S11 parameter graphic is obtained (see Figure 3.16). It can be seen that with the new parameter configuration the expected wideband properties are obtained around the wanted frequencies, which are located in the 800-1000 MHz band and 1800-2000 MHz band. Also, the ripples presented in the upper band from Figure 3.12 are now smoother.

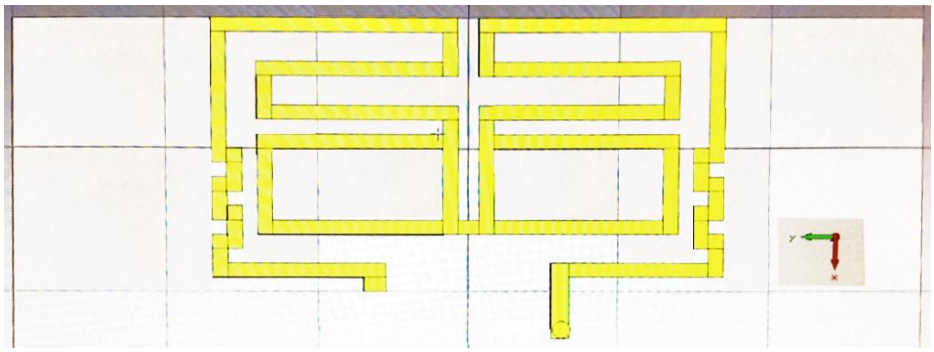

Figure 3.15. First antenna redesign.

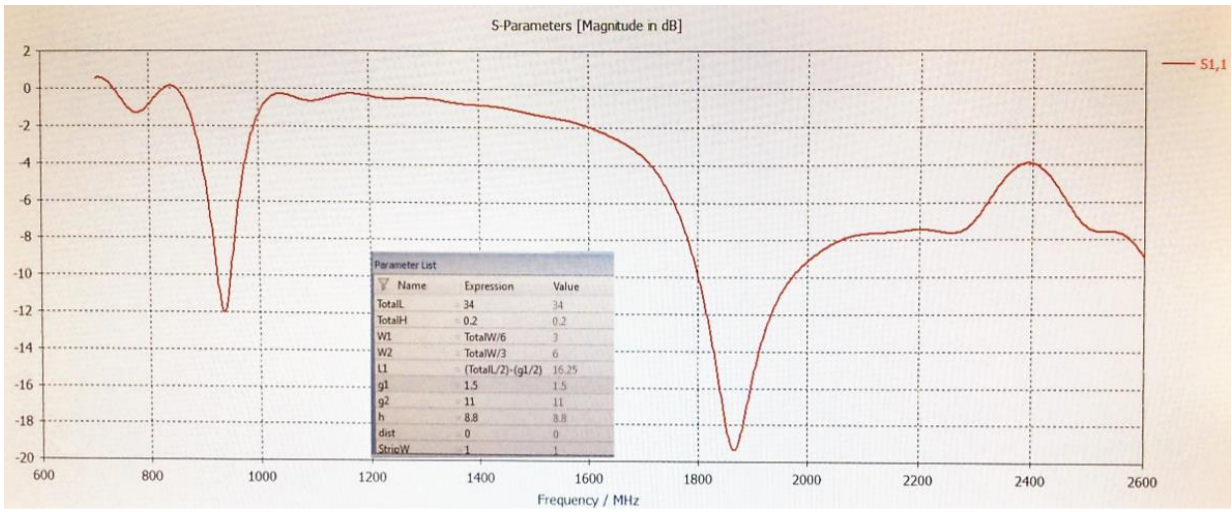

Figure 3.16. S11 parameter after the first optimization.

3.1.4. Second approach

In this second procedure, the current basic design that works properly and meets the requirements is transformed in order to achieve “Company 1” existing solution’s performance while fulfilling the company´s requisites for our proposed antenna.

Firstly, the “Company 1” schematic (see Figure 3.17) where the antenna will be placed, determines the new substrate and copper ground plane dimensions. Thus, the current substrate size is 60(L) x 85(W) mm2, which includes the space where the antenna is located. The current copper ground plane size is 60(L) x 85(W) mm2 minus the width of the antenna, which is 18(W) mm prior optimization, giving a total of 60(L) x 67(W) mm2. The copper ground plane width is, therefore, dynamic, and changes depending on the current antenna width, which will be modified along with the other parameters to fit the established requirements.

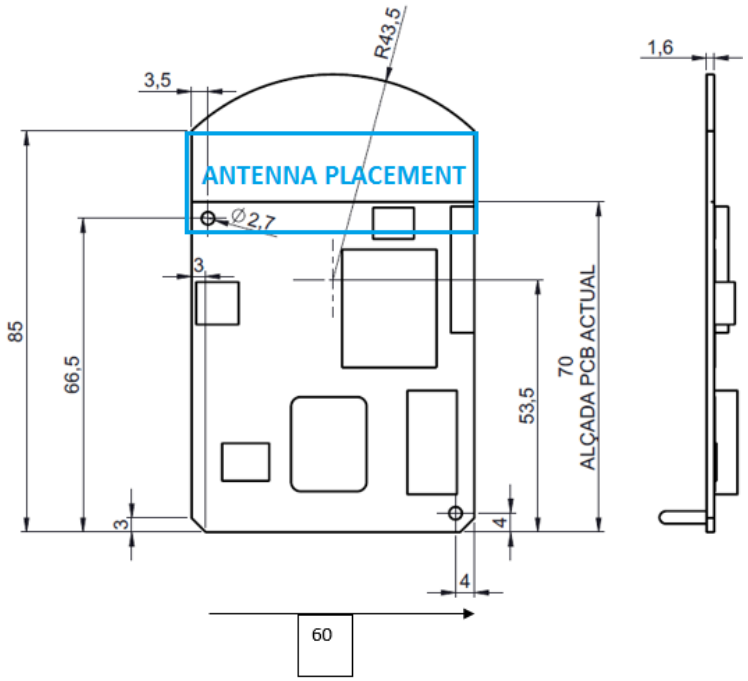

Figure 3.17. Schematic PCB module for the proposed antenna.

Secondly, another major change that takes place is the integration of the device's casing, filled with resin, which also modifies the reflexion coefficient result of the antenna performance. The resin material has a relative permittivity Er= 3 and a tangent loss of 0.04.

As expected, the first simulation of the second approach does not comply with the requirements set by the existing solution behaviour (see Figure 3.18) and, for this reason, we directly move on to the next optimization iteration.

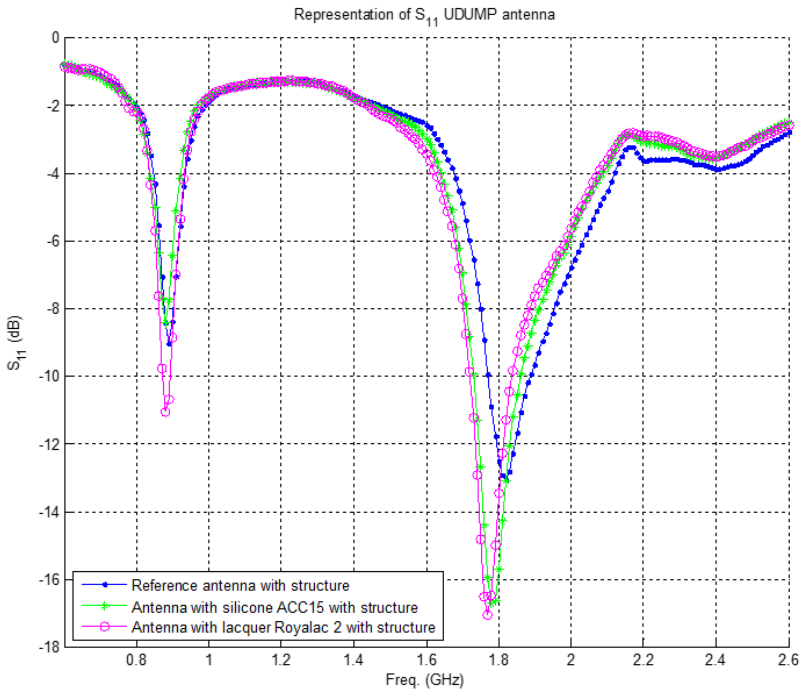

Figure 3.18. "Company 1" S11 real tested results for the existing solution with different protections.

3.1.5. Second optimization

Following the steps taken in "First optimization", several parameter combinations were tried, applying the before mentioned rule (*New_L= Current_L*Current_freq/ Desired_freq*) as a guideline to place the resonant frequencies in their desired place along with a trade-off between the other design values.

However, in this case, it was not possible to find a suitable performance within the given design (see Figures 3.19 and 3.20) from the second approach, as the final simulation (see Figure 3.21) shows by not meeting the requirements of Figure 3.18.

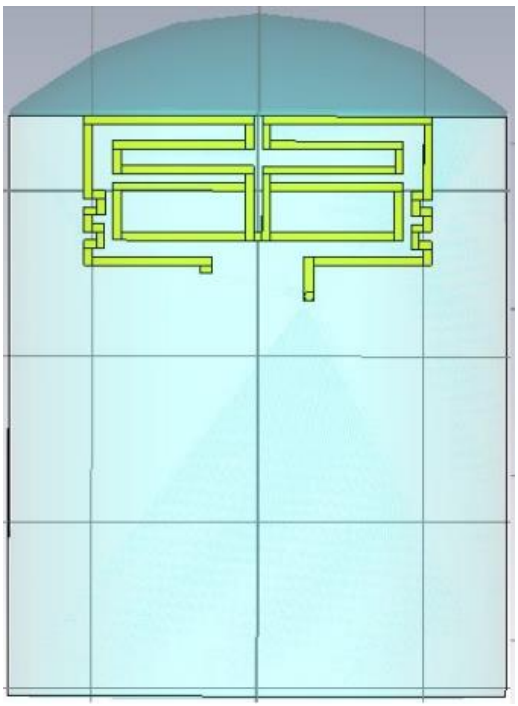

Figure 3.19. Second optimization approach, complete front part of the dual-loop antenna design.

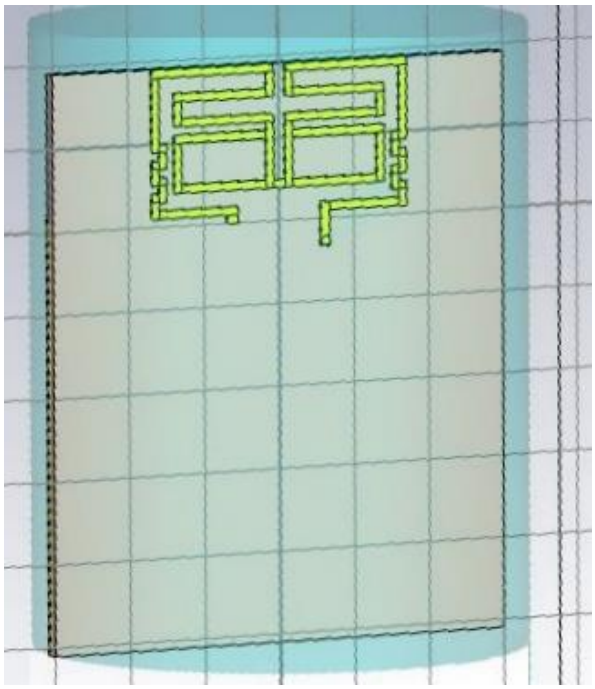

Figure 3.20. Second optimization approach, front lateral part of the dual-loop antenna design.

Figure 3.21 represents the best overall performance that could be found regarding the reflection coefficient during the second optimization stage. It was acquired by giving to each of the next listed parameters the subsequent measures:

- Antenna Total Length= 58 mm.
- Antenna Total Width= 18 mm (same value as before).
- g1= 2 mm.
- g2= 15 mm.

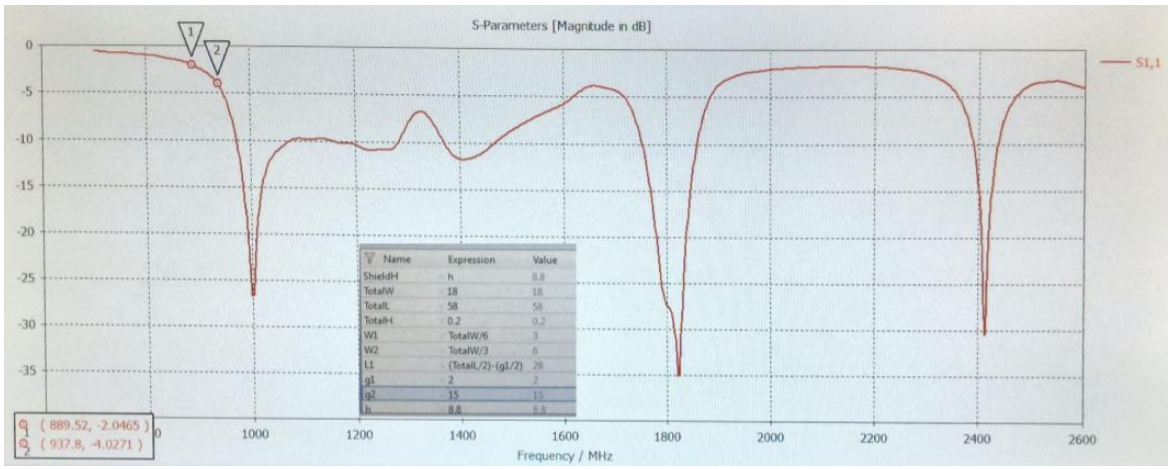

Figure 3.21. S11 parameter after the second optimization.

As a consequence, it was decided to split up the optimization task by aiming at obtaining first the low band resonant frequency, leaving the achievement of the upper band resonant frequency for the following subchapter.

Obtaining our first goal (see Figure 3.22), by moving down in frequency (around 900 MHz) the low band antenna operation point situated at 1000 MHz in figure 3.21, was relatively easy to obtain. The new values for the design parameters are:

- Antenna Total Length= 56 mm.
- Antenna Total Width= 22 mm.
- g1= 1 mm.
- g2= 14 mm.

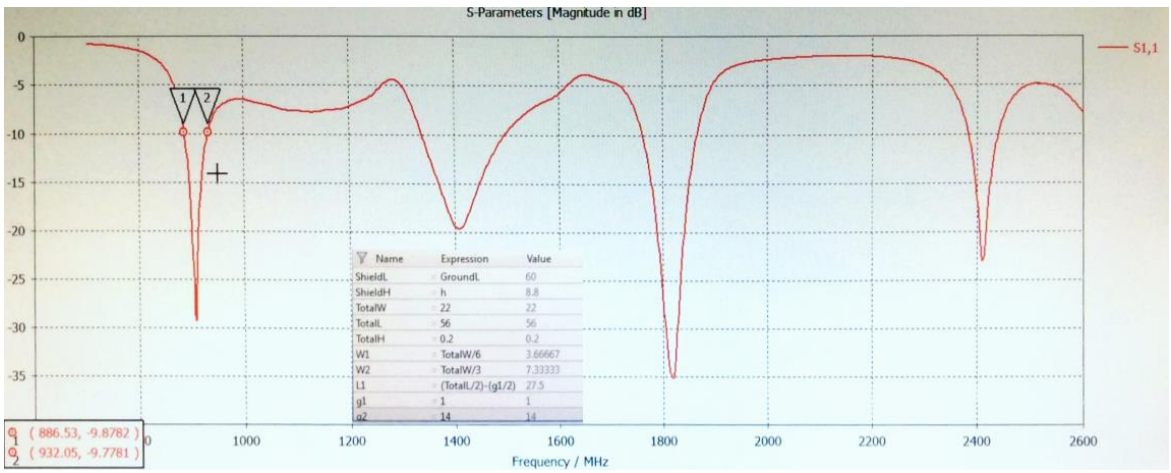

Figure 3.22. S11 parameter achieving low band operating point.

The most difficult part, meeting the specifications in the upper frequency band without significant ripples, is a challenge that will be overcome in the following paragraphs.

3.1.6. Third optimization

To completely obtain the desired results, we went one step further by analysing the currents that take place in the antenna, which emerge from the H-plane coaxial's TEM mode. Placing monitors in the frequencies from figure 3.22 that we want to get rid of, such as the highest one at 2400 MHz, allows seeing in red colour (see Figure 3.23) the antenna strips where the current flows are more intense. Those are the ones we should redesign to achieve a suitable behaviour.

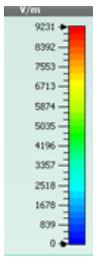

Figure 3.23. Coloured scale for current intensity from the feeding cable to the antenna structure.

Thus, it could be observed that the strips corresponding to the paths E and G, were causing the unwanted performance, they had intense currents at the undesired frequencies. Once this information was available, we proceeded to eliminate the corresponding strips and simulate the new structure (see Figures 3.24, 3.25, 3.26 and 3.27).

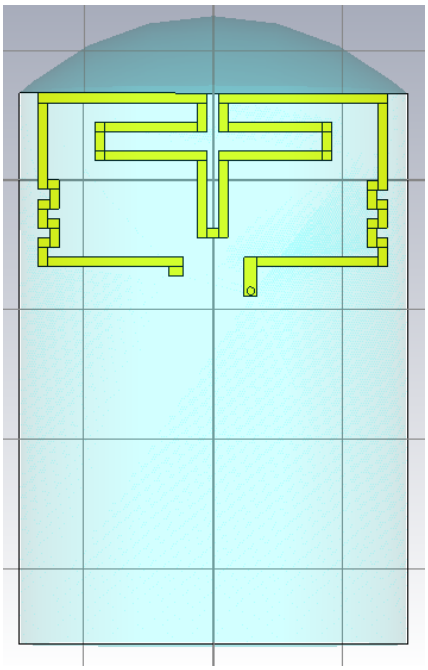

Figure 3.24. Third optimization approach, complete front part of the antenna design.

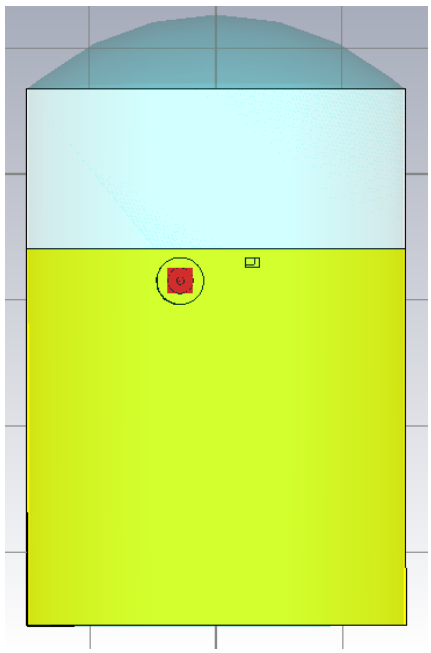

Figure 3.25. Third optimization approach, complete back part of the antenna design.

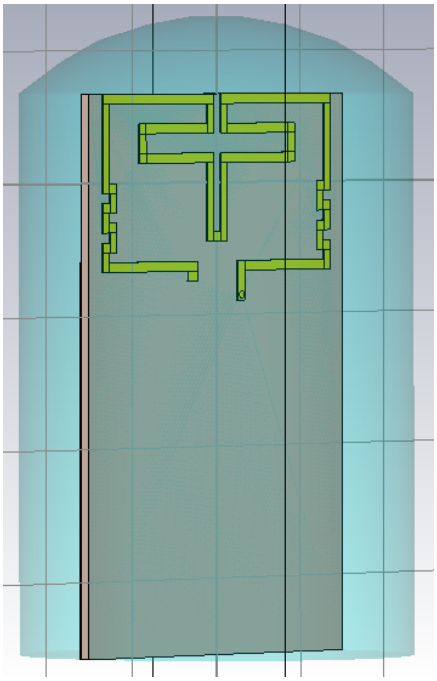

Figure 3.26. Third optimization approach, front lateral part of the antenna design.

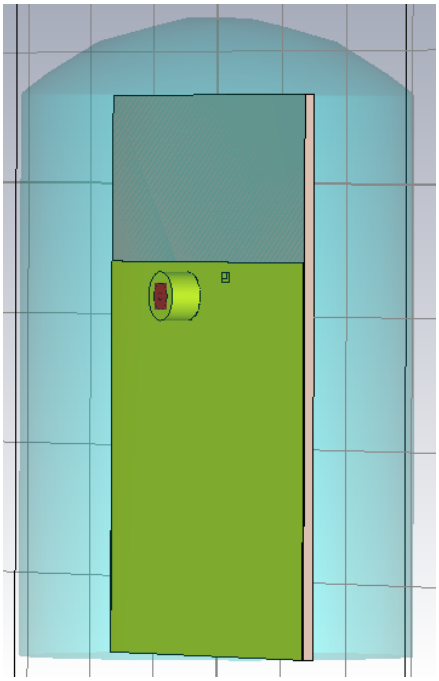

Figure 3.27. Third optimization approach, back lateral part of the antenna design.

3.1.6.1. Useful rules for optimization

When carrying out the simulations in the redesigned antenna, two useful statements can be derived and employed any time with, at least, this new proposed antenna. Thus, for the remain strips that compose the antenna's inner loop, whose path corresponds to D and H from Figure 3.3, the following rules apply (see Figure 3.28):

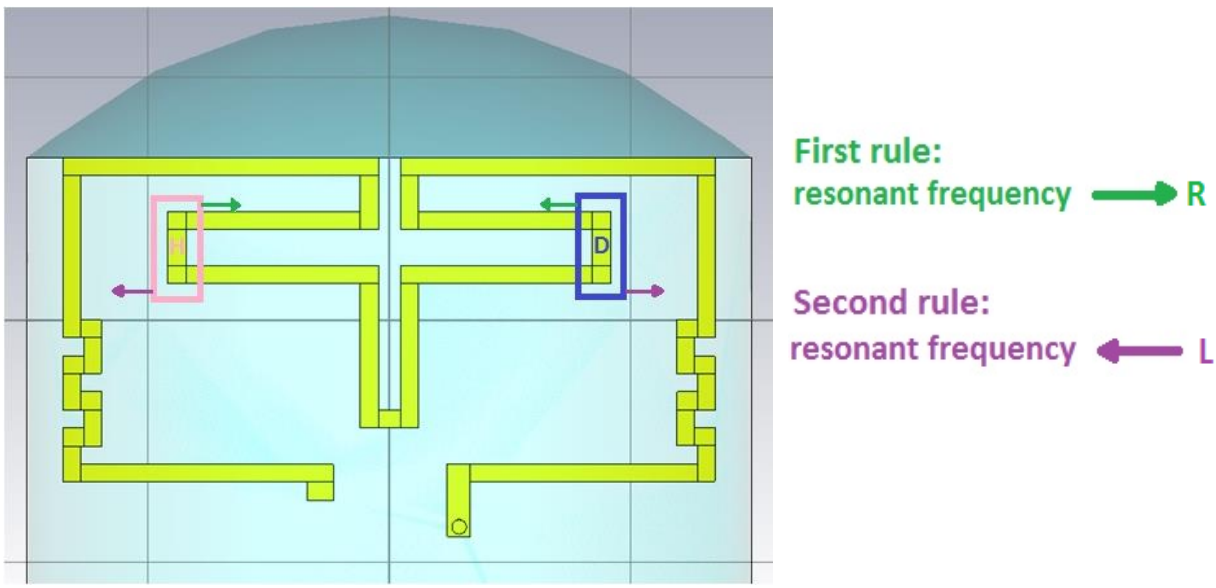

Figure 3.28. Schematic: Antenna new structure optimization rules.

- First rule: the more the vertical strip is moved from path D to the left, along with the symmetrical movement of the vertical strip H to the right, the resonant frequency of the upper band moves proportionally to the right (the upper band operational frequency increases) in the S11 graphic.
- Second rule: the more the vertical strip is moved from path D to the right, along with the symmetrical movement of the vertical strip H to the left, the resonant frequency of the upper band moves proportionally to the left (the upper band operational frequency decreases) in the S11 graphic.

3.2. Final antenna design and optimization

Applying the second and third optimizations along with an overall improvement, by considering the impact of modifying the rest of the parameters' values, led to the following design characteristics (see Figure 3.29):

- Antenna Total Length= 54 mm.
- Antenna Total Width= 26.8 mm.
- g1= 1.8 mm.
- g2= 9.2 mm.

Name	Expression	Value
GroundH	0.2	0.2
GroundL	60	60
GroundW	70	70
SubsH	1.6	1.6
SubsW	GroundW	70
SubsL	GroundL	60
ShieldW	GroundW	70
ShieldL	GroundL	60
ShieldH	h	8.8
TotalW	26.8	26.8
TotalL	54	54
TotalH	0.2	0.2

W1	TotalW/6	4.46667
W2	TotalW/3	8.93333
L1	(TotalL/2)-(g1/2)	26.1
g1	1.8	1.8
g2	9.2	9.2
h	8.8	8.8
dist	0	0
StripW	1	1
StripH	0.2	0.2
L1_aux	L1/(49/6)	3.19592
CoaxBack	1.5	1.5
CoaxL	5	5
Coax_r	0.6	0.6
CoaxR	2.01	2.01
CoaxR3	3.71	3.71

Figure 3.29. Parameter list used for the final antenna design.

This final optimization process took place as follows:

- First, based on the third optimization structure, it was found that for a 2.4 mm difference in distance to the left for path D and right for path H (First rule), the main specifications were approximately achieved, such as the resonant frequency points and a good radiation performance. Thus, both the low-band and upper-band resonant frequencies were accomplished.

- Next, for the fixed width and length values from the second optimization (56 mm and 22 mm), the g1 and g2 values were modified accordingly to exactly achieve the antenna´s operational point with no ripples in the high frequencies.
- Last but not least, the width and length values were slightly modified to finally meet the best possible fractional bandwidth (see Figure 3.30).

The consequent final antenna´s reflection parameter (S11) appears in the next figure:

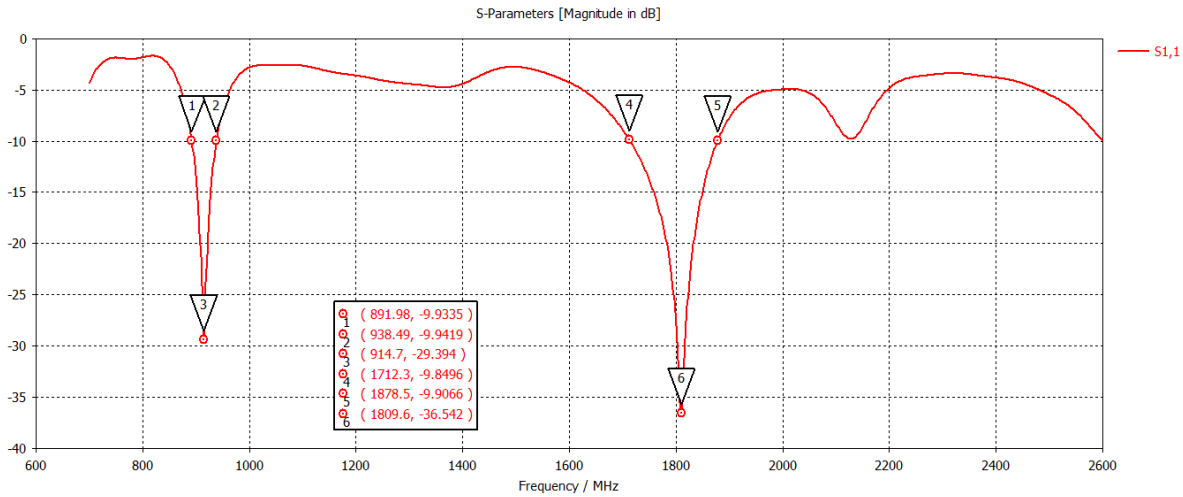

Figure 3.30. S11 parameter for the final antenna design.

From the image, it is possible to determine the two main resonant frequencies of the antenna that meet the desired specifications, which are 914.7 MHz and 1809.6 MHz (number 3 and 6 respectively, from Figure 3.30). Moreover, the antenna Q can be estimated by measuring the 10 dB return loss fractional bandwidth (FBW):

$$Q = fc/(f2-f1) = 1/FBW$$

Therefore, for the lower frequency band → Q= 914.7/ (938.49 - 891.98)= 19.67

and for the upper frequency band → Q= 1809.6/ (1878.5 - 1712.3)= 10.89.

It should be noticed that antennas with a high Q are narrowband and, antennas with a low Q are wideband. The higher the Q value, the more sensitive the input impedance is to small changes in frequency.

3.2.1. Final antenna performance without its casing

Even though the final antenna implementation consists of an embedded PIFA within a PCB module surrounded by a resin casing, it is useful to simulate the behaviour

of the antenna itself in order to know whether the fabrication prototype will work accordingly when examined with a vector network analyser (Agilent), before adding the device module's material. The final antenna structure without resin for the simulation is hereafter:

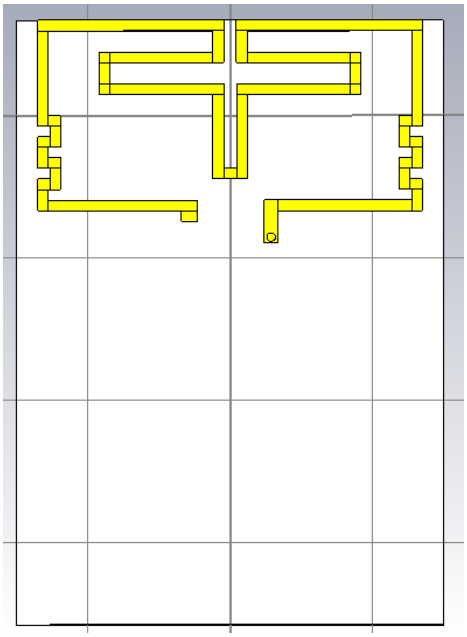

Figure 3.31. Final front part of the antenna design without casing.

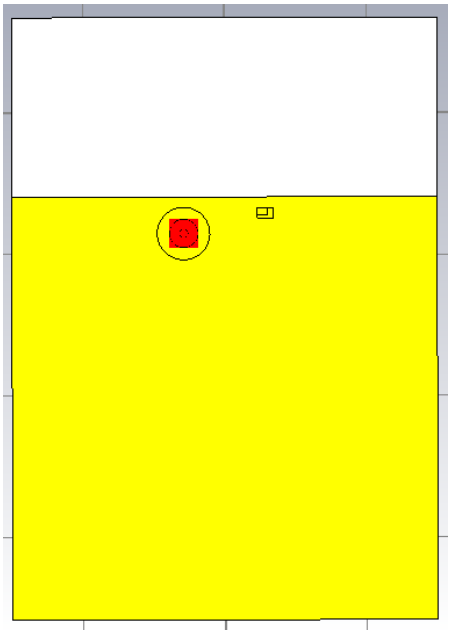

Figure 3.32. Final back part of the antenna design without casing.

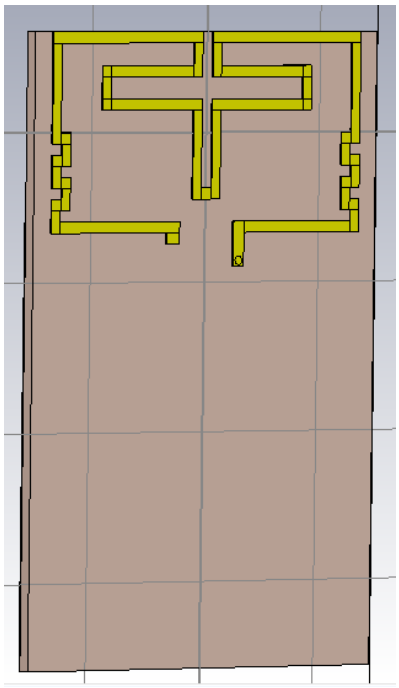

Figure 3.33. Final front lateral part of the antenna design without casing.

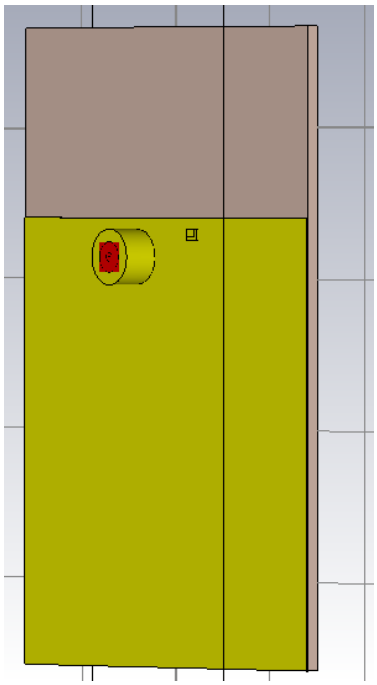

Figure 3.34 Final back lateral part of the antenna design without casing.

which corresponds to the interior of Figures 3.24, 3.25, 3.26, 3.27 (no casing, just the antenna device).

The presented dual-loop compact antenna simulation (see Figure 3.35) has two main resonant frequencies in the bands 800-1000 MHz and 1200-1400 MHz, which shows how the absence of the casing produces a frequency decrement in the operating points, especially in the upper band.

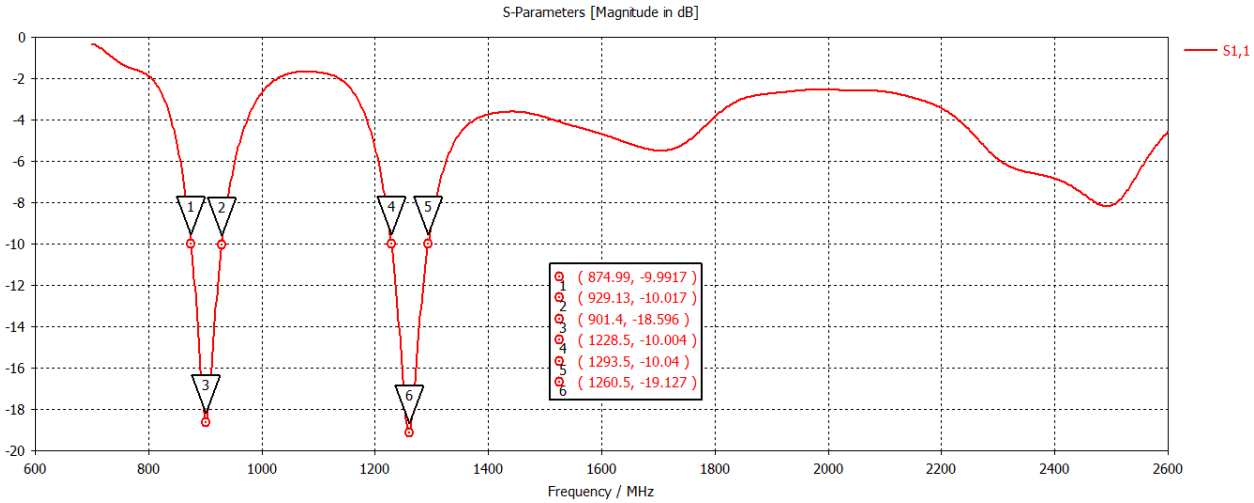

Figure 3.35. S11 parameter for the final antenna design with no resin.

This performance is what we will be looking for when testing the antenna structure after its fabrication and, after adding the resin surrounding, it should be leading to the desired results.

4. Fabrication process

4.1. Antenna fabrication and its specifications

The antenna fabrication based on our final CST Microwave Studio design involves a series of steps prior its realization.

First of all, the fabrication process requires neither taking every single measure from the antenna structure nor delimiting them in the layout. By simply exporting the CST model to an Autocad (see Figure 4.1) or Gerber format, the information required is obtained.

In our case, a Gerber format was employed for the laboratory technicians to be able to print the design. Going to the modelling menu in CST, the export 2D (two dimensions) option to Gerber was chosen (see Figure 4.2).

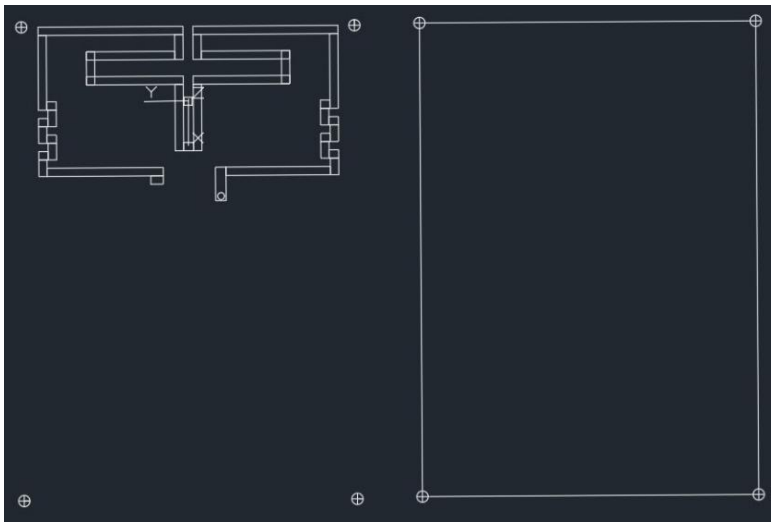

Figure 4.1. Autocad model result exported from CST.

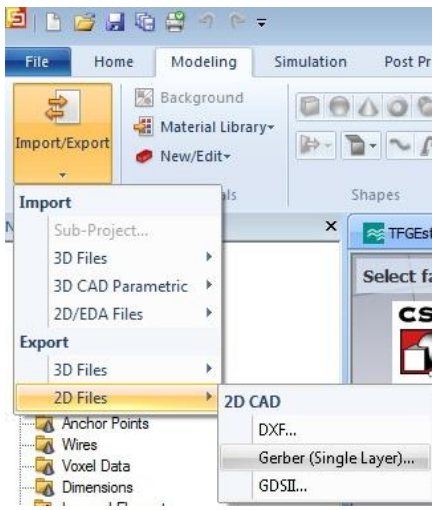

Figure 4.2. How to export from CST to Gerber format in 2D.

Next, in order to have all the copper layers visualized correctly, four markers in each corner of the substrate were placed from the corner to the outside (see Figure 4.3). This is needed in order to know where to cut when placing the printed layers on top of each other.

The resulting bottom and front layers with the Gerber extension (.gbr) can be visualized online (see Figure 4.4).

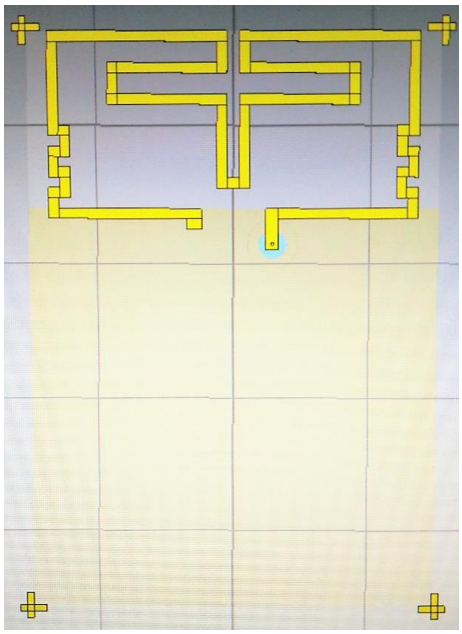

Figure 4.3. Antenna final design with markers on the substrate's corners.

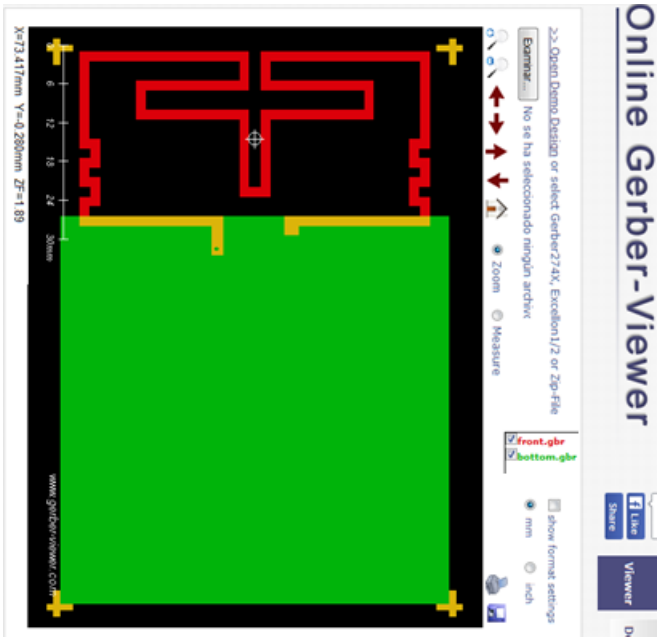

Figure 4.4. Front.gbr and bottom.gbr from our antenna design.

In Figure 4.4, the red and green layers belong to the front and back part of the presented antenna respectively. The intersections between both layers, such as the four markers, the antenna strip that connects to ground and the antenna strip that connects to the coaxial feeding cable, are represented in yellow.

In order to get the bottom.grb and front.grb printed, a photoplotter was employed, which is primarily used in Integrated Circuits' packaging and for the production of PCBs (printed circuit boards), like in our case. The printed images are, therefore, the guide for a specialized machine to know where to eliminate the copper from a square of the substrate dimensions. Finally, the resultant front mask goes on top of the substrate, placing at the bottom the other respective mask with a coaxial cable to feed the antenna.

With respect to the substrate, the flame retardant FR4 material (also called: Glass reinforced epoxy laminated sheets) was chosen (see Figures 4.5 and 4.6); the reasons for its ubiquity as a PCB material are its high mechanical and dielectric strength, resistance to humidity, and light weight among other favourable properties with regard to PCB manufacturing. Despite knowing that its dielectric constant doesn´t keep its value throughout the substrate surface, for our purpose it is suitable to use. This is because, when dealing with strips, it acts as a proper supporter. However, when dealing with microstrip antennas where the substrate is used for propagation purposes, FR4 should be replaced by other type of substrates that are more reliable in practice and actually maintain their dielectric constant at the same value along all the surface, such as Rodgers 4003c.

Figure 4.5. FR4 material (taken from www.alibaba.com).

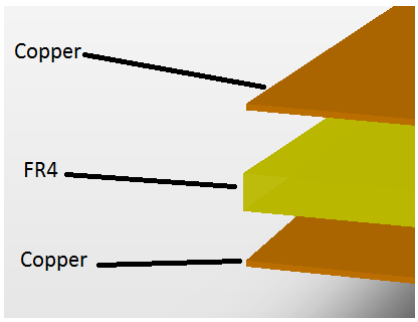

Figure 4.6. PCB layer description (taken from www.blackstick.co.uk).

Figure 4.7. SMA Female connector taken from (www.lowpowerlab.com).

4.1.1. Deviations from simulation to fabrication

Unlike in the simulated design, the fabricated antenna contains a 1-mm-diameter inner coaxial cable. The connector type is a SMA (SubMiniature version A) (see Figure 4.7) with a 50 Ω impedance, and its 'hot' terminal welded to the track. Also, the hole where the coaxial cable connects is countersunk in order to prevent a shortcircuit in the groundplane. The final antenna prototype for the proposed compact dual-loop antenna is shown in Figures 4.8 and 4.9:

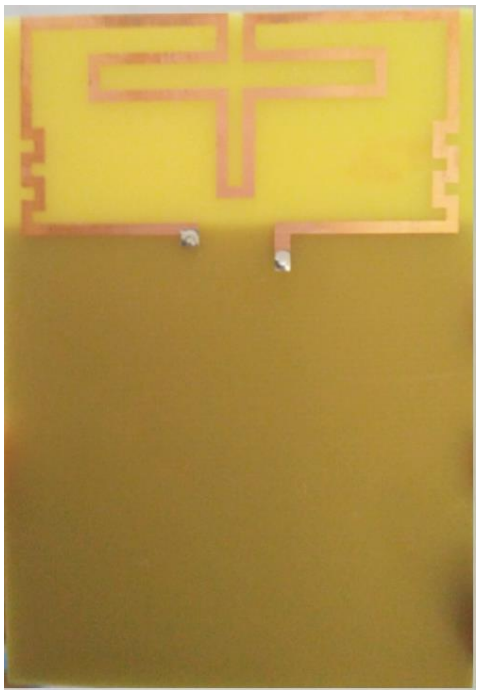

Figure 4.8. Front part of the fabricated dual-loop antenna design.

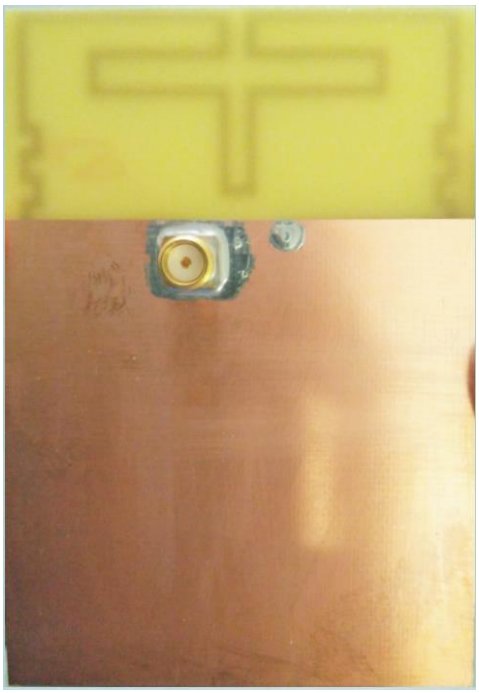

Figure 4.9. Back part of the fabricated dual-loop antenna design.

Additionally, the antenna prototype is placed into its casing and filled in with resin, as it will be implemented in practice (see Figure 4.10).

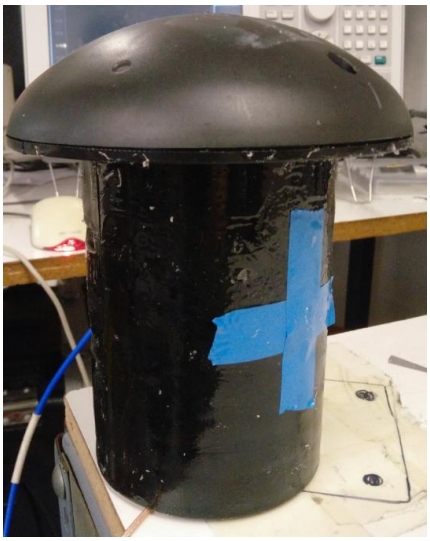

Figure 4.10. Completed antenna prototype (with the resin casing), fabricated at UPC University, Catalonia, Spain.

4.2. Environmental impact

The potential, benefits and applications of the Internet of things, such as our proposed embedded antenna in a sensor device, is a well-known fact among professionals in the high tech industry.

The impact of IoT on social life and manufacturing has been welcomed by everyone nowadays due to the easiness and convenience of using cloud-connected cars, smart supply chain processes, intelligent wearables, and so on, integrated in our daily lives.

4.2.1. IoT environmental drawbacks

Studies forecast that by 2020 there will be nearly 26 billion items deployed worldwide, raising big environmental concerns around the growth of the IoT and the sensors´ recycling process. Within few years, the current generation of IoT devices will become obsolete due to an enhancement in the hardware upgrades along with hundreds of modern IoT items entering the market.

The exponential growth in IoT electronics, which are replete with a variety of heavy metals and synthetic chemicals, leads to an e-waste disposal of non-biodegradable and fairly new products that usually end up being incinerated or placed in regular landfills when recycled.

In addition to this accelerated replacement cycle, the energy consumption constitutes another challenge, which takes place in the production of sensor devices and the big data centers in charge of supporting the IoT networks.

4.2.2. IoT environmental advantages

On the other hand, IoT has great positive impacts. Going beyond IoT healthcare applications or its positive social changes, the use of this technology in order to track the physical environment is leading to promising facts.

Nowadays, it enables environmental innovative solutions such as reducing the air pollution with smart parking projects, saving energy by using motion sensors in intelligent streetlights, factories' emissions monitoring, or reducing water loss through leakages controls. The information gathered by these projects and implemented sensors proves to be beneficial not only for our surroundings but for people working in hazardous settings like firefighters, policemen, or workers in radiation prone environments; allowing for a better understanding and preparation when finding solutions to risky situations.

4.2.3. Project environmental impact

First of all, the small size of the IoT final product saves a lot more space and material that the already existing solutions, contributing to a mayor benefit in the recycling process due to the scalability of the project.

Installing smart embedded technology in garbage containers provides with safer and more efficient haulers' work. Not only can they change their transport route dynamically, saving energy and polluting less by reducing the CO2 emissions, but also they are informed on time in case any accident or fire is detected near the containers.

To sum up, when fabricating an antenna for an IoT product, the material properties and its performance need to be taken into consideration in order to provide with a sensor device that can function correctly as many years as possible, and that could be reused for other system applications.

5. Results

After the antenna's fabrication, the next step is to test whether the obtained simulation results can be validated in practice. By means of an Agilent's Vector Network Analyser (VNA), the performance of the fabricated final antenna proposed in this project is compared with Company 1's existing solution and its competitor (Company 2's approach). These distinctions are also drawn when measuring the antennas' radiation diagrams in the anechoic chamber for the frequency range of interest.

5.1. Vector Network Analyser outcomes

5.1.1. Antenna without resin

As mentioned before, we will first test the presented antenna without casing to verify to which extent the fabrication process has influenced the simulated antenna's behaviour. The results obtained for our implemented antenna are the following:

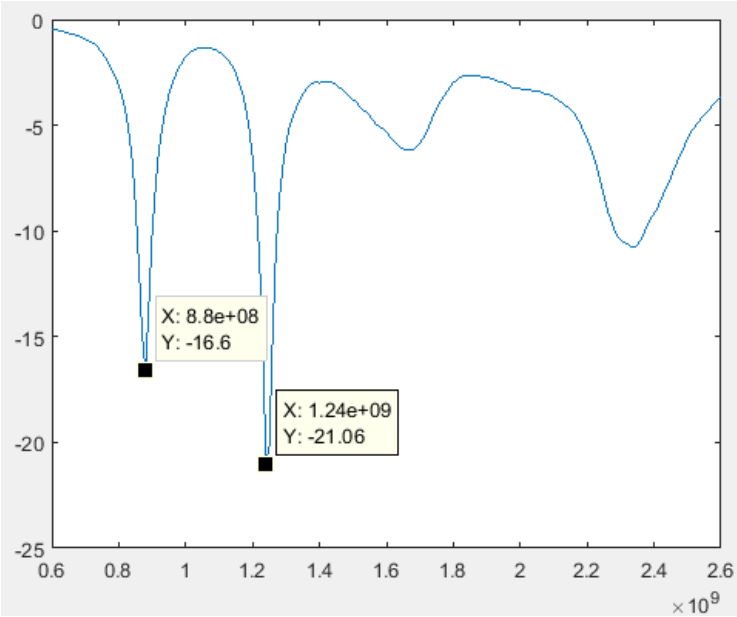

Figure 5.1. S11 parameter for the fabricated final antenna.

where the 'x' axis corresponds to the frequency range in Hz and the 'y' axis to the S11 parameter magnitude in dB. As we can see in Figure 5.1, the two main resonant frequencies are placed at 880 MHz and 1240 MHz, which, in comparison with their simulated equivalent (see Figure 3.35) are close to the required values, differing an

amount of 20 MHz each. This ensures the accuracy of the obtained simulated results in analysing the antenna performances using the simulation software. For this reason, it is expected to obtain similar values to the simulation results with a frequency shift of 20ish MHZ regarding the complete antenna prototype (with the casing effect).

5.1.2. "Company 1" actual antenna

In Figure 3.18, the performance of the existing solution inside a casing structure that we try to enhance at a lower cost, and from which we specified the desired requirements is presented. However, we took the measurements at the university laboratory from the antenna itself, without any material structure, obtaining the next results:

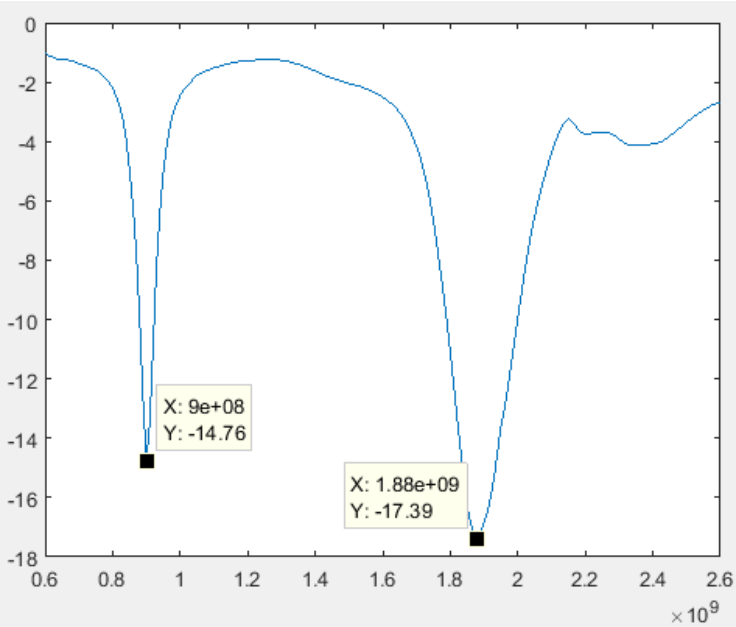

Figure 5.2. S11 parameter for the "Company 1" actual antenna.

In Figure 5.2, it can be observed that our test results carried out in practice match the test results followed during the design approach for the low band, with an 80 MHz increment for the upper frequency band compared to Figure 3.18. Yet, if we compare this result with the proper equivalent VNA graphic of the antenna itself (see Figure 5.3), we can see that the resonant frequency values match perfectly to the "Silicone ACC15 without structure". This comes to show that the 80 MHz difference between the tested results in the upper band is due to the material effect that surrounds the antenna, which highly influences the overall performance of the device as we can see.

In Figure 5.3, the comparison between antenna scenarios is made for both the antenna and the antenna inside a structure. In this case, although the S11 parameters of the antenna with silicon and lacquer have been shifted to lower frequencies, the two GPRS (General Packet Radio Service) bands are still covered.

In the first band, which goes from 824.2 MHz to 960 MHz, the displacement in frequency is not significant since the antenna with silicone covers the band well. But in the second band, even though the displacement in frequency is larger, the band is still covered from 1710 MHz to 2170 MHz.

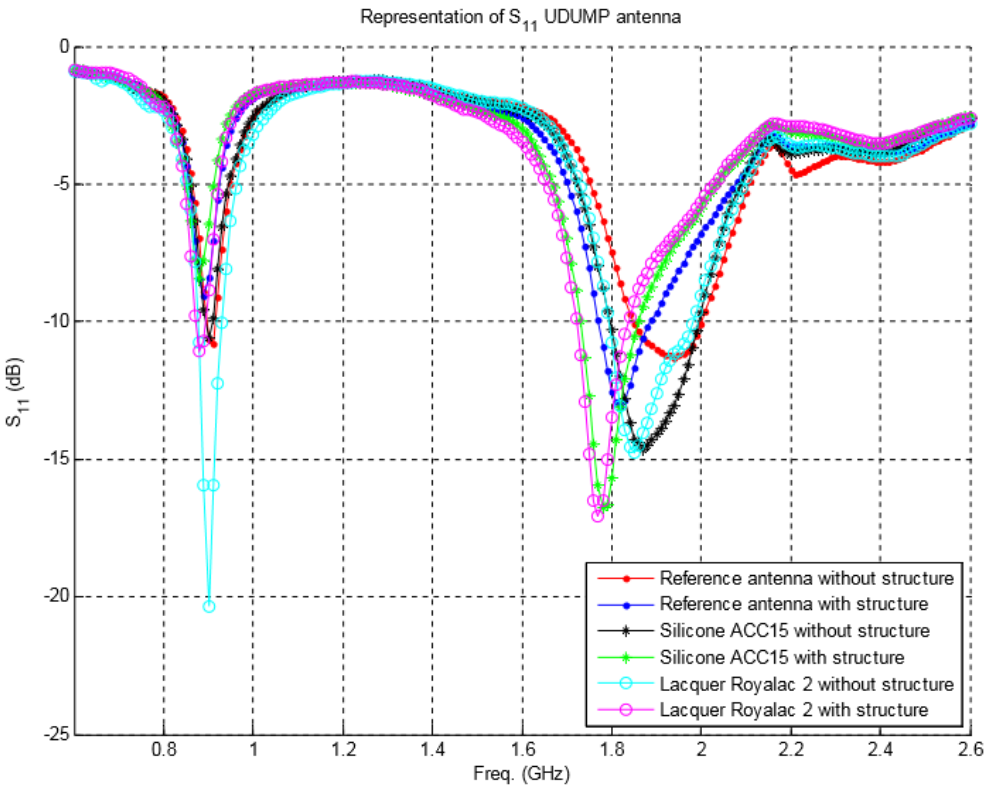

Figure 5.3. "Company 1" VNA S11 results for the existing solution with and without different protections.

5.1.3. "Company 2" actual antenna

The competition antenna's behaviour is shown in Figure 5.4. It should be noticed the wide 10 dB return loss bandwidth in the upper band, and the two main resonant frequencies at 830 MHz and 1920 MHz. Even though the overall performance is similar to "Company 1" existing solution, covering the specific frequency range for mobile communication, "Company 2" antenna has the advantage of a smaller size since it is a PCB module instead of two separated devices (one for the antenna that transmits the information and the other for the sensor that gathers the data).

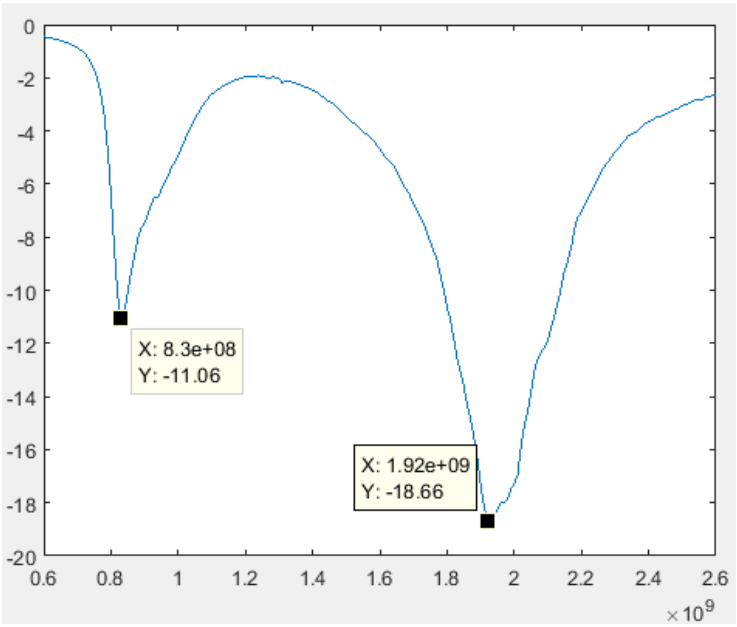

Figure 5.4. S11 parameter for the "Company 2" actual antenna.

5.1.4. Antenna with resin

Finally, we collected the VNA test results for the complete proposed final antenna, which was covered in resin inside the previously defined structure (see Figure 4.10).

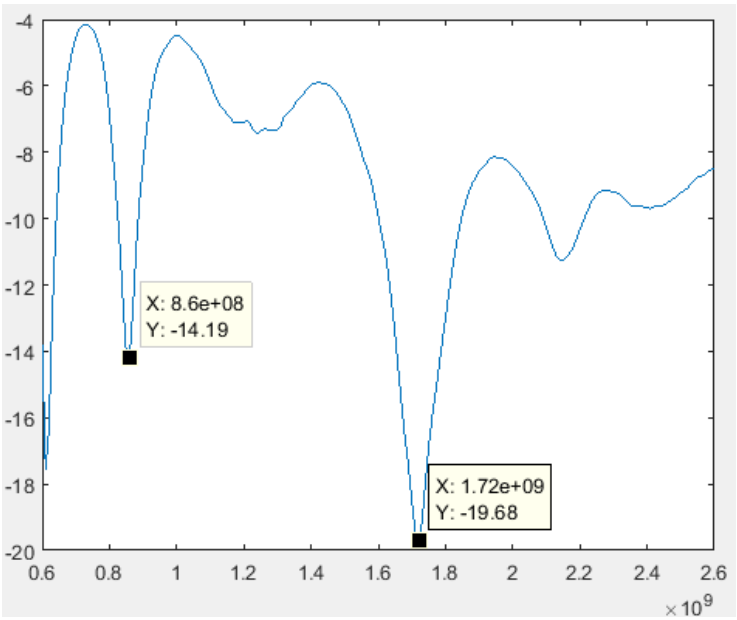

Figure 5.5. S11 parameter for the complete presented antenna.

The graphic obtained (see Figure 5.5) shows two operational frequency points at 860 MHz and 1720 MHz, with a good 10 dB return loss impedance bandwidth, which covers well enough the requested frequency range for a proper information transmission.

Thus, the antenna's bandwidth suits the mobile wireless communication systems GSM and DCS, fulfilling the goal proposed at the beginning of this project ("to have resonant frequencies in the bands 800-1000 MHz and 1700-1900 MHz, suitable to be integrated within sensors") with a more compact and affordable antenna than the existing solutions.

On the other hand, even though the fabricated antenna with resin is a considerably good first practical approach that meets the requirements and easier to produce than other antennas, there is still room for improvement. Better results can be achieved in the next iteration, which is explained in the sixth paragraph when discussing about the future development.

5.2. Anechoic chamber outcomes

An anechoic chamber is an echo-free room designed to completely absorb reflections of either electromagnetic waves or sound (see Figure 5.6), they are also insulated from exterior sources of noise. They simulate a quiet open-space of infinite dimension, which is useful when exterior influences would give false results otherwise.

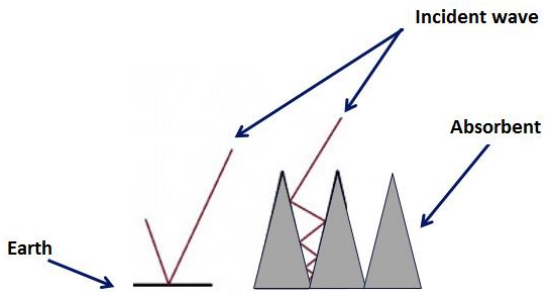

Figure 5.6. Anechoic chamber effect.

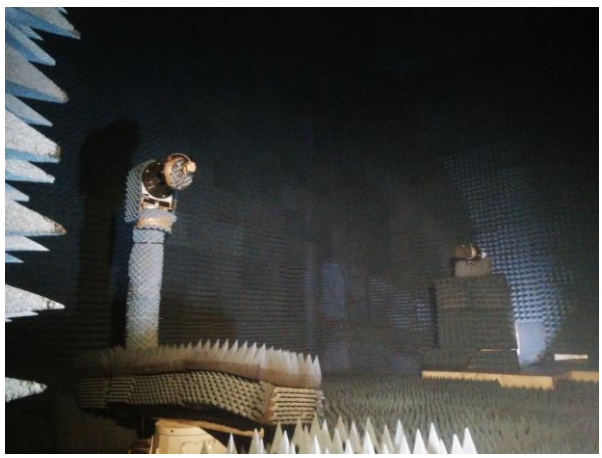

Figure 5.7. Anechoic chamber at UPC University, Catalonia, Spain.

Hence, the anechoic chamber is used to measure the antenna's behaviour in a controlled environment. They can measure radiation diagrams from 800 MHz to 40 GHz, transform the near field to far field and measure in cylindrical and spherical coordinates.

The chamber dimensions where the antennas were tested (see Figure 5.7) are: 10 m x 7,5 m x 6 m, so 450 m^3 of volume. All measures can be done in remote way to do not disturb signals. The resultant radiation diagrams obtained from measuring "Company 1" actual antenna, "Company 2" actual antenna, and the proposed antenna with resin are shown in the appendix (section 7).

5.2.1. Comments on the results

All in all, fairly omnidirectional patterns have been obtained in the phi plane over the three selected frequencies that matter for the mobile communication standard, indicating a good agreement between the experimental and theoretical results.

In the proposed antenna with resin, it is confirmed that the antenna is relatively omnidirectional even in the higher frequencies where the pattern becomes more complex. This quasi omnidirectional pattern is obtained due to its symmetrical structure, which results in the minimum degradation of the radiation pattern at specific angles. Moreover, this is the desirable performance of an antenna designed for IoT purposes where the radio-base location is not determined and the antenna ought to be responsive anywhere as much as possible.

5.2.1.1. Directivity measures

Table 5.1 shows the directivity values at all the frequencies that matter for the proposed and existing solutions.

The directivity of the three different solutions varies in some dB. As it can be seen, our proposed antenna shows better directivity for the lowest and highest bands in comparison with the existing solutions, being on average between "Company 1" and "Company 2" actual antenna for the second highest band, which is an overall great result.

Antenna	Frequency in MHz	Directivity in dB
Actual antenna "Company 1"	900	3,41
Actual antenna "Company 1"	1790	5,58
Actual antenna "Company 1"	2000	4,91
Actual antenna "Company 2"	850	3,18
Actual antenna "Company 2"	1930	3,68
Actual antenna "Company 2"	2150	4,02
Antenna with resin	850	6,04
Antenna with resin	1720	4,83
Antenna with resin	2150	6,68

Table 5.1. Directivity measures of the analysed antennas (“Company 1” actual antenna, “Company 2” actual antenna, and our proposed antenna with resin), at three different frequencies.

5.2.1.2. Gain and efficiency measures

Antenna	Freq in MHz	Gain in dB	Efficiency in dB
Actual antenna "Company 2"	850	-0,18	3,36
Actual antenna "Company 2"	1930	2,247	1,433
Actual antenna "Company 2"	2150	2,55	1,47
Antenna with resin	850	-0,11	6,15
Antenna with resin	1720	1,2	3,63
Antenna with resin	2150	0,37	6,31

Table 5.2. Gain and efficiency measures in dB of the “Company 2” actual antenna and our proposed antenna with resin, at three different frequencies.

For the three main frequencies, the gain and efficiency values are shown in dB in Table 5.2 for both the proposed and “Company 2” solutions.

It can be observed that the gain obtained for our antenna with resin is lower than for the existing solution at the upper frequency band but higher for the low frequencies.

The reason behind the lower gain is that the resin filling inside the presented antenna`s casing structure generates losses that the other antenna does not have. However, these losses are justified due to the fact that it is necessary to protect the antenna structure against the environmental impact it may experience. Thus, when applied in IoT solutions, the proposed antenna will be able to work well during longer periods of time than unprotected antennas employed in similar purposes.

Furthermore, the proposed antenna´s efficiency in this project is much higher when compared with the one from “Company 2" actual antenna (the already marketed competitor´s solution).

Therefore, by having a more efficient antenna than the competition and taking into account all the measures from section 5, it can be concluded that a good realization of an alternative to the already marketed antennas, at a low cost and with the required performance, has been achieved. This proves the theoretical study successful and achieves the goals proposed in section 1.4. “Project scope”.

6. Conclusions and future development

6.1. Thesis conclusion

A compact dual-loop antenna for multiband operation that complies with the GSM and DCS mobile communication standards, to be integrated properly within sensor devices, is analysed and proposed in this project.

This PIFA antenna contributes to achieve as good results as the already marketed solutions, with the advantages of a reduced size and cost of fabrication. In comparison with previous studies, the presented antenna allows for an easy operating frequency tuning to compensate the casing effect from the sensor device.

When implementing and testing the investigated antenna, proper directivity and radiation features were achieved, improving on general terms the existing solutions' behaviour taken as a role model.

For these reasons, the proposed antenna design with a wide 10 dB return loss impedance bandwidth is well suitable for integration into various IoT sensor devices to meet GSM/DCS applications.

6.2. Future development

Despite achieving a good first approximation to our expectations, some improvements can be done in order to be even closer to the desired performance results.

As described in Section 3.1.4, the resin material that fills the device structure has a relative permittivity Er= 3 and a tangent loss of 0.04, which affects the final results as observed in Section 5.1.1. As a consequence, the antenna's behaviour can be improved by using the exact right value for the relative permittivity in the simulations and optimize the antenna with the same casing effects that the fabricated prototype will experience after the implementation process.

The way to achieve so will consist on modifying the resin's relative permittivity until we get an S11 graphic that complies with the antenna with resin test results for the VNA (see Figure 5.2). Once the exact Er value is known, we can proceed to optimize the antenna by changing slightly some parameters as it was done in Section 3.1.5 and 3.1.6 until we get the desired resonant operating frequencies.

7. Appendix

7.1. "Company 1" actual antenna

At 900 MHz:

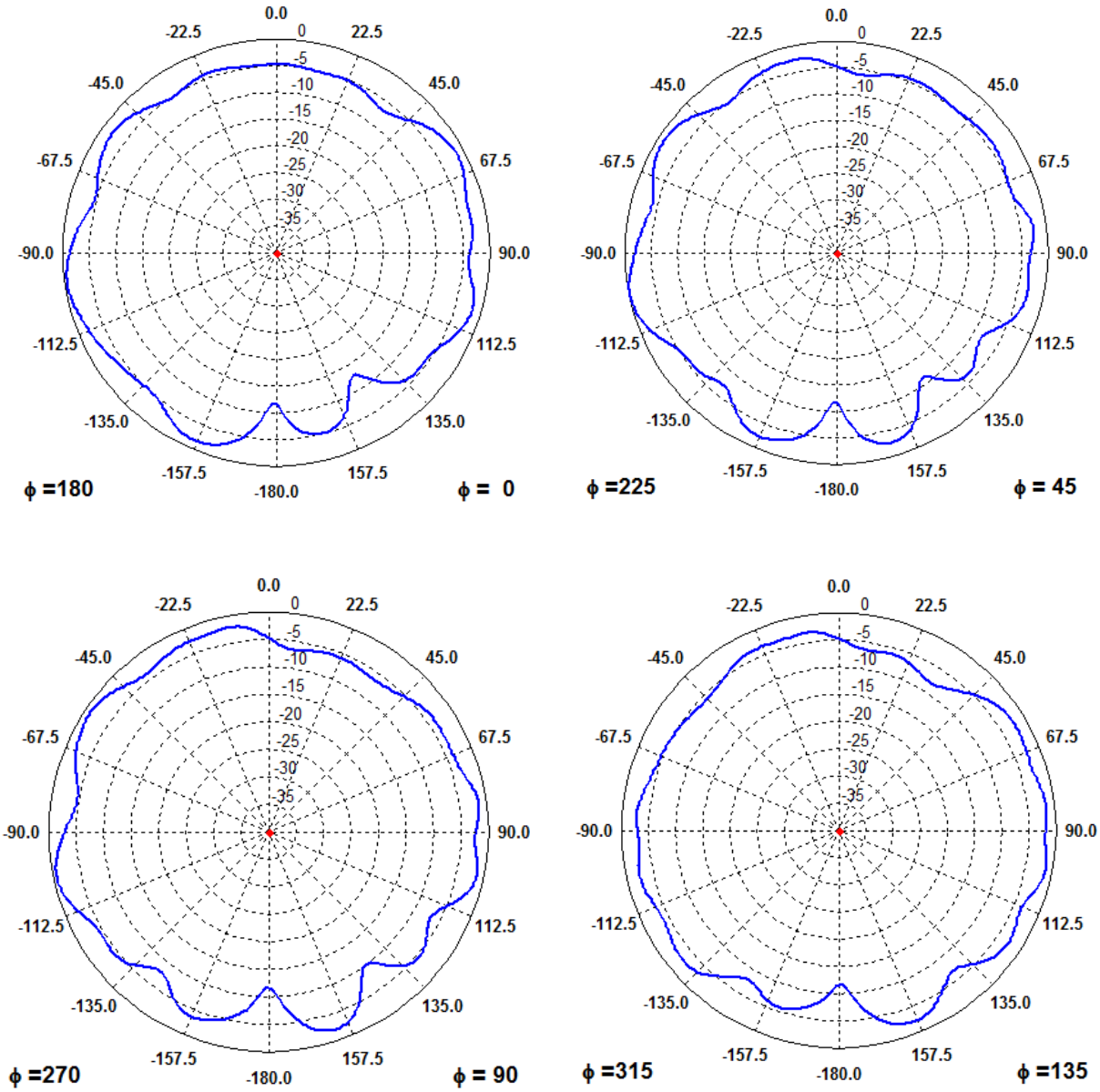

Figure 7.1. Radiation pattern cuts at 900 MHz of the "Company 1" actual antenna.

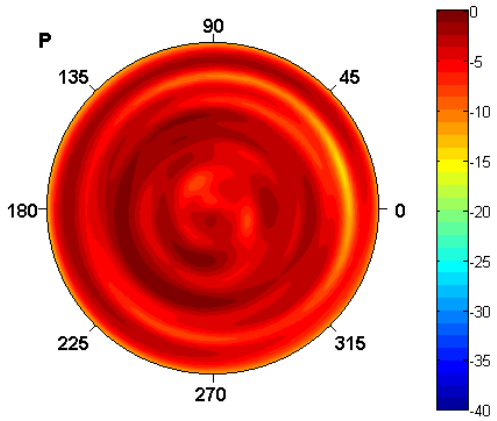

Figure 7.2. "Company 1" actual antenna front view of the radiation pattern at 900 MHz.

At 1790 MHz:

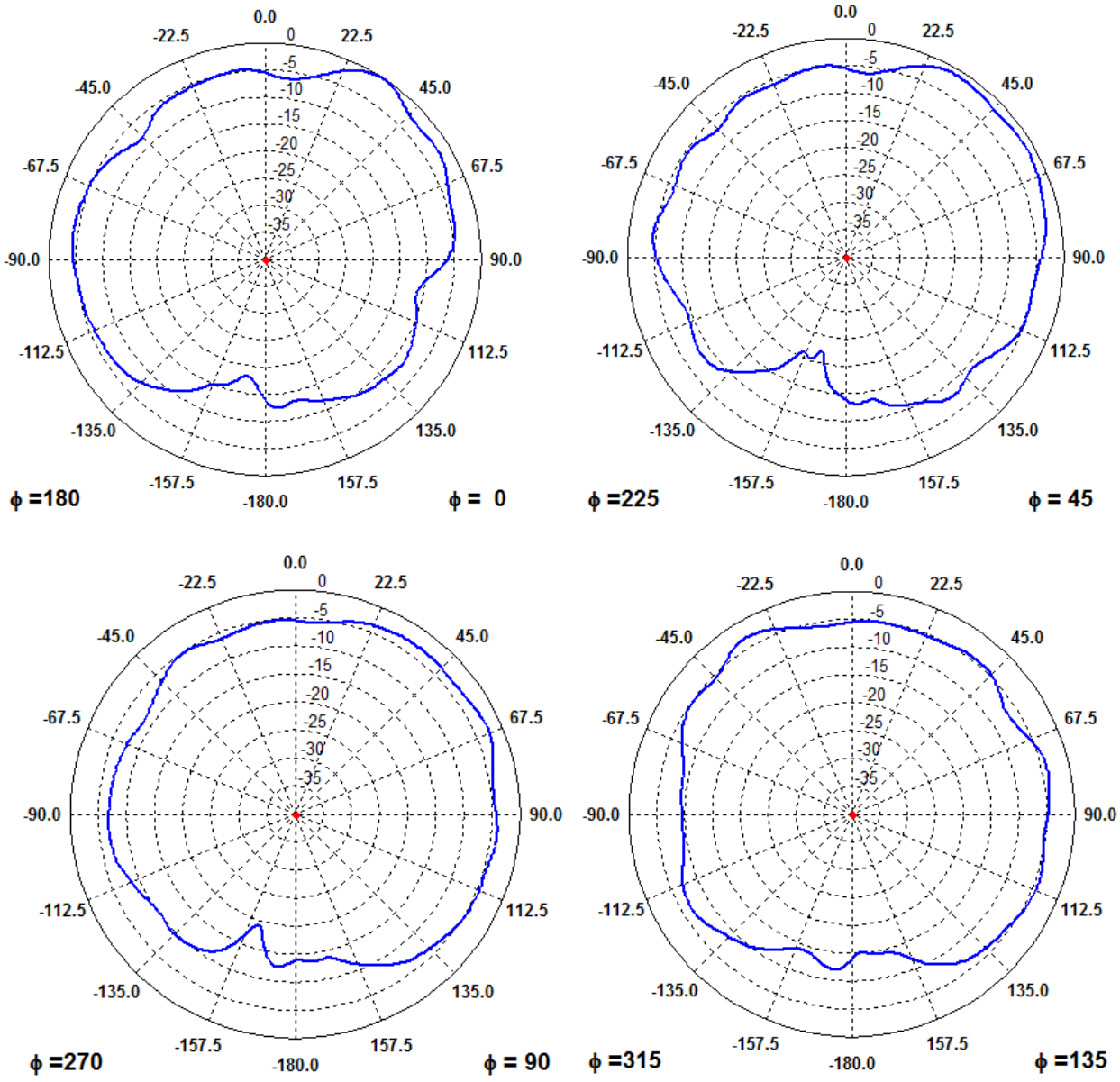

Figure 7.3. Radiation pattern cuts at 1790 MHz of the "Company 1" actual antenna

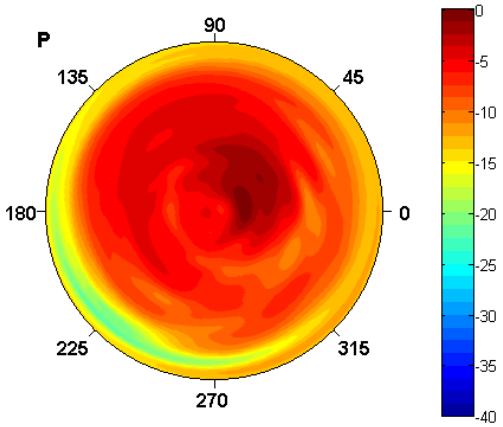

Figure 7.4. "Company 1" actual antenna front view of the radiation pattern at 1790 MHz.

At 2000 MHz:

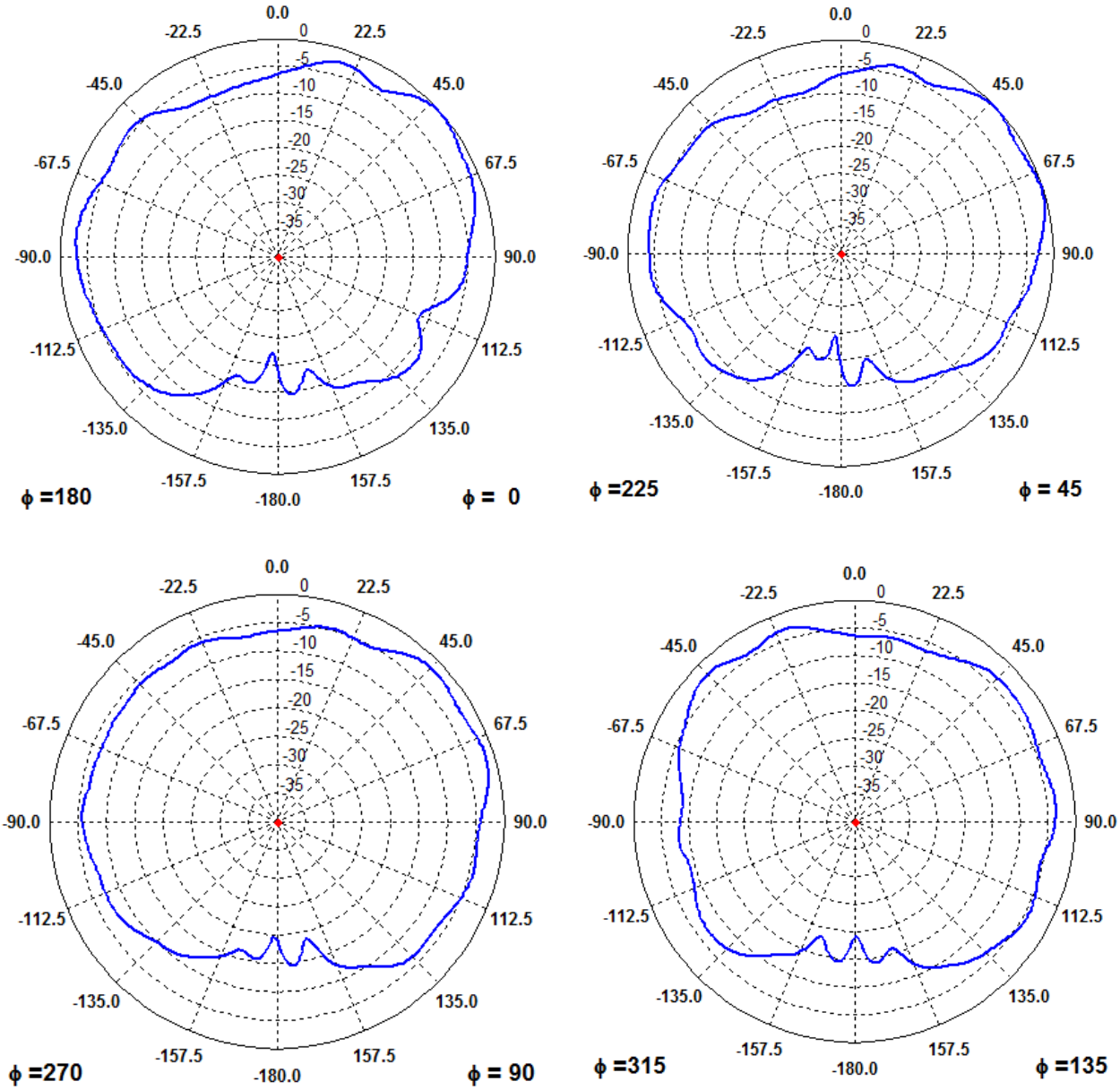

Figure 7.5. Radiation pattern cuts at 2000 MHz of the "Company 1" actual antenna.

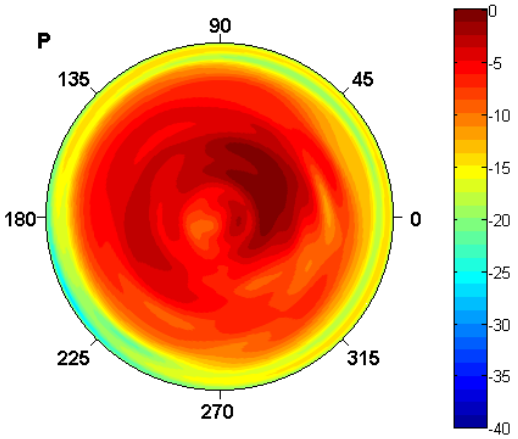

Figure 7.6. "Company 1" actual antenna front view of the radiation pattern at 2000 MHz.

7.2. "Company 2" actual antenna

At 850 MHz:

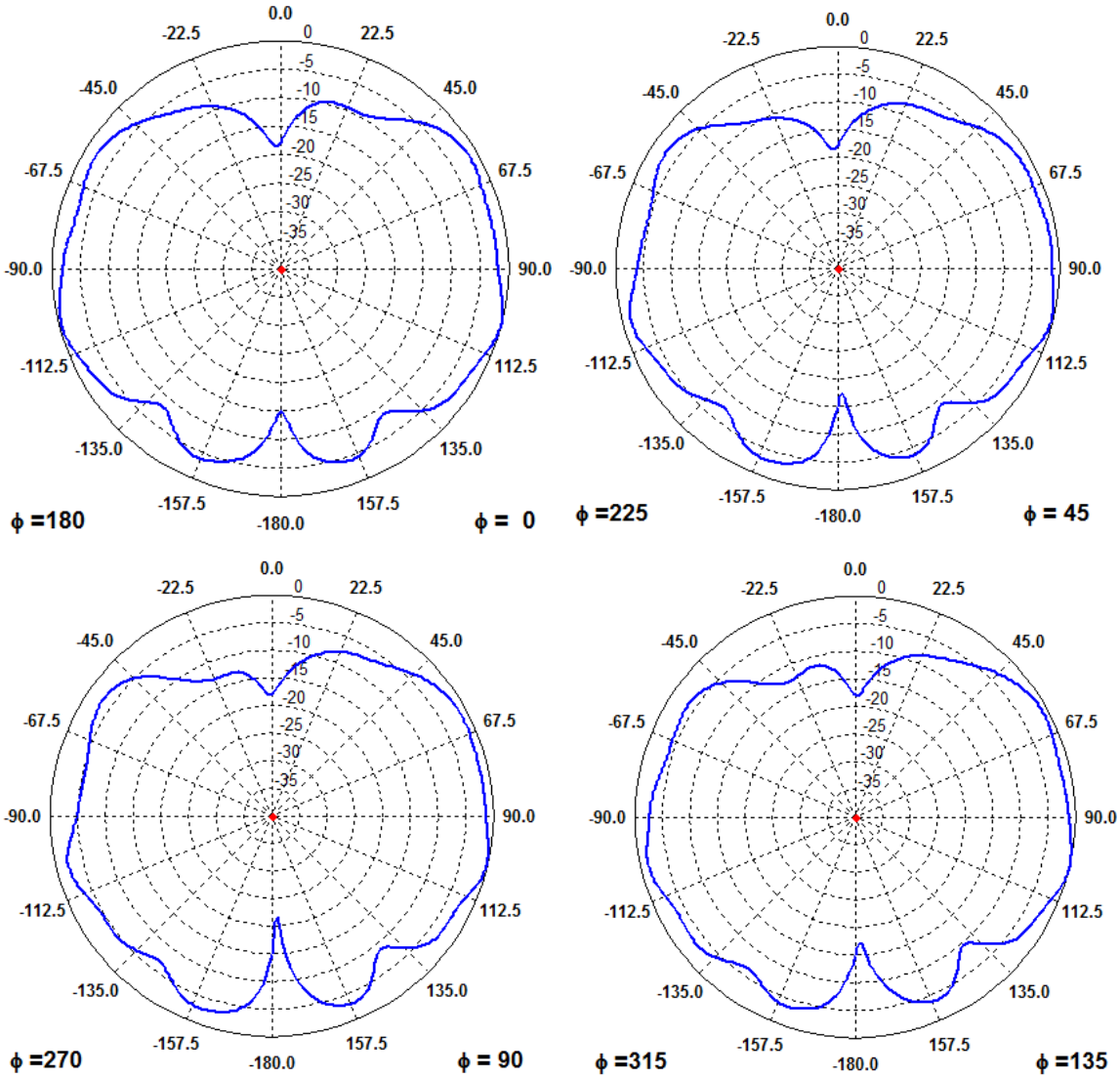

Figure 7.7. Radiation pattern cuts at 850 MHz of the "Company 2" actual antenna.

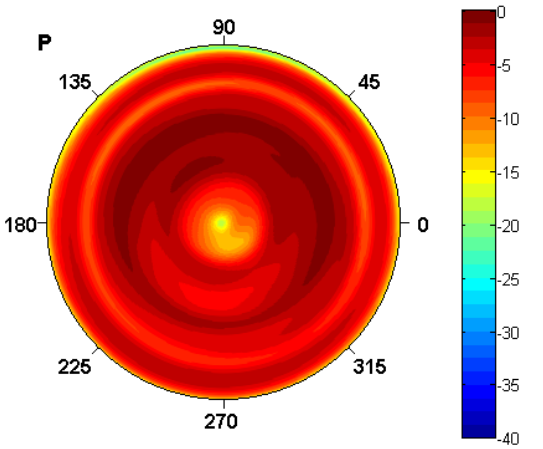

Figure 7.8. "Company 2" actual antenna front view of the radiation pattern at 850 MHz.

At 1930 MHz:

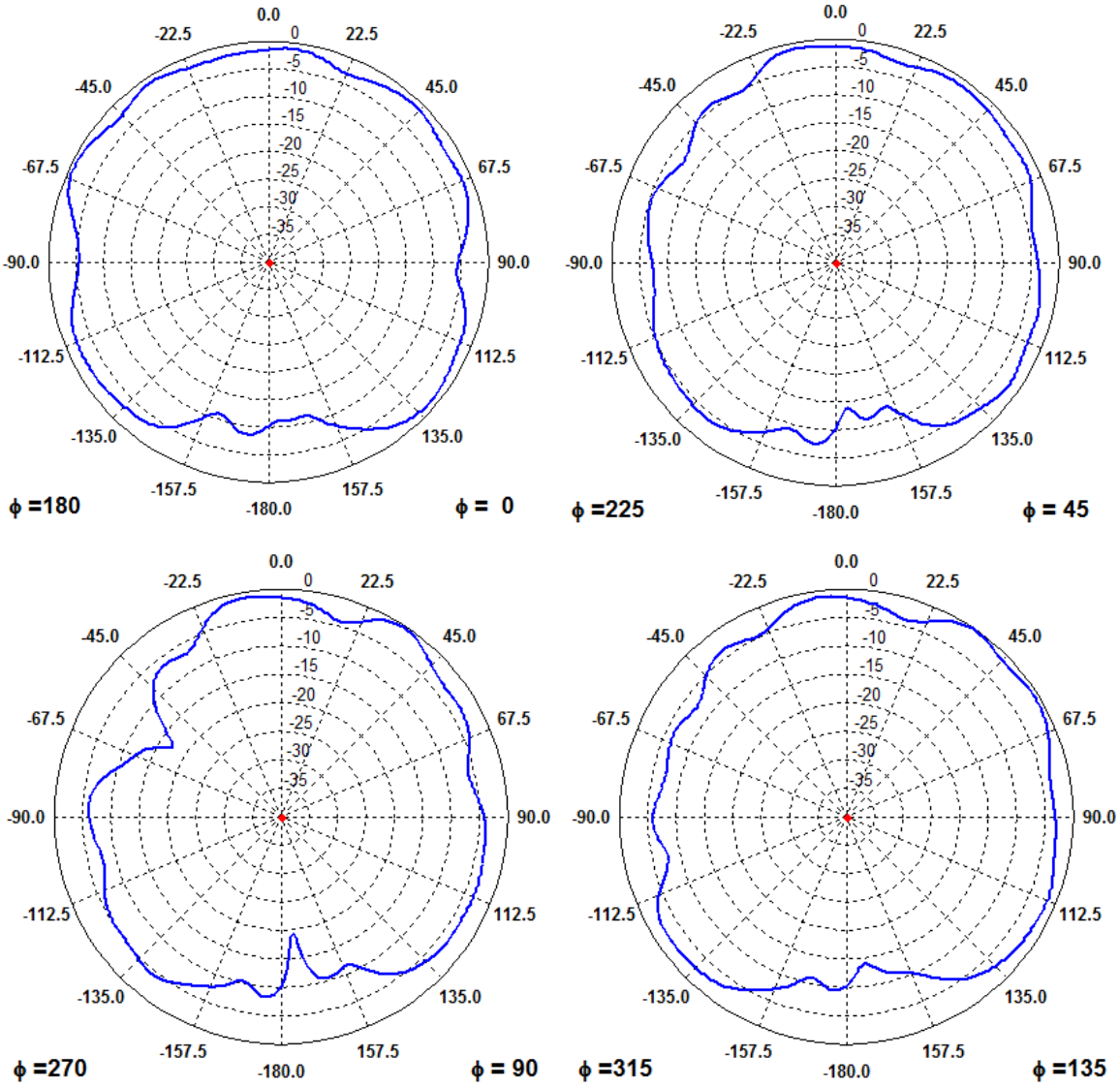

Figure 7.9. Radiation pattern cuts at 1930 MHz of the "Company 2" actual antenna.

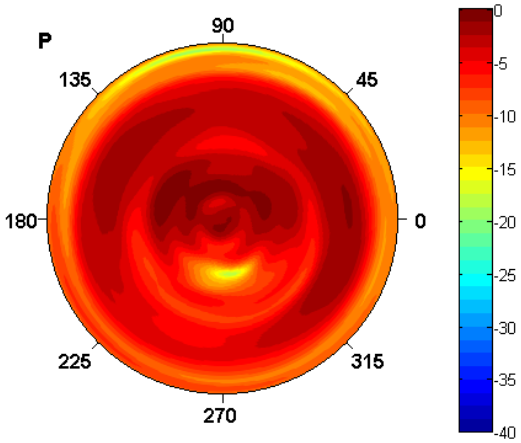

Figure 7.10. "Company 2" actual antenna front view of the radiation pattern at 1930 MHz.

At 2150 MHz:

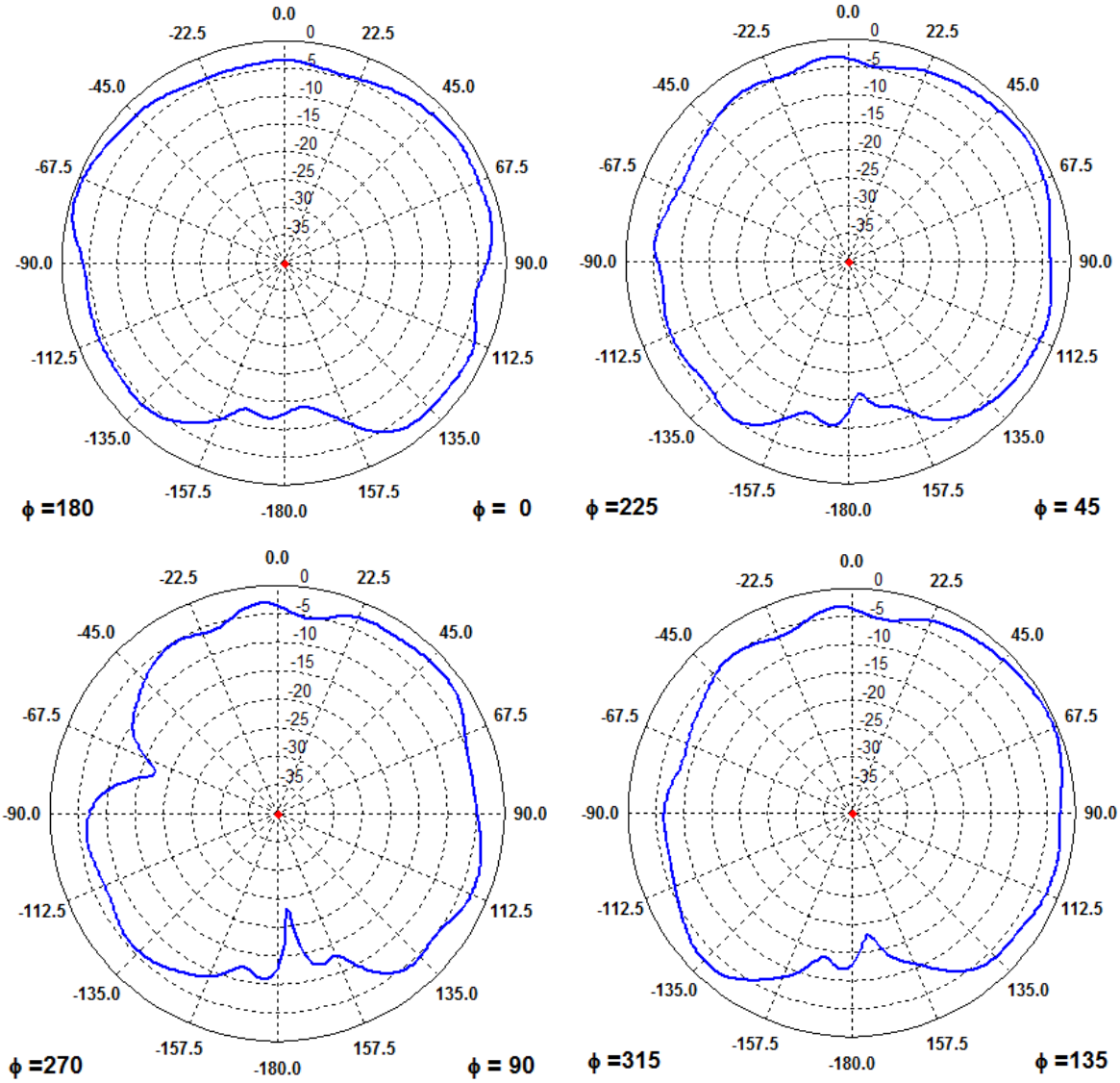

Figure 7.11. Radiation pattern cuts at 2150 MHz of the "Company 2" actual antenna.

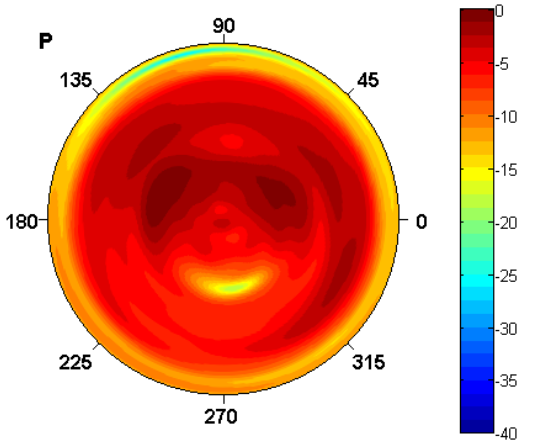

Figure 7.12. "Company 2" actual antenna front view of the radiation pattern at 2150 MHz.

7.3. Antenna with resin

At 850 MHz:

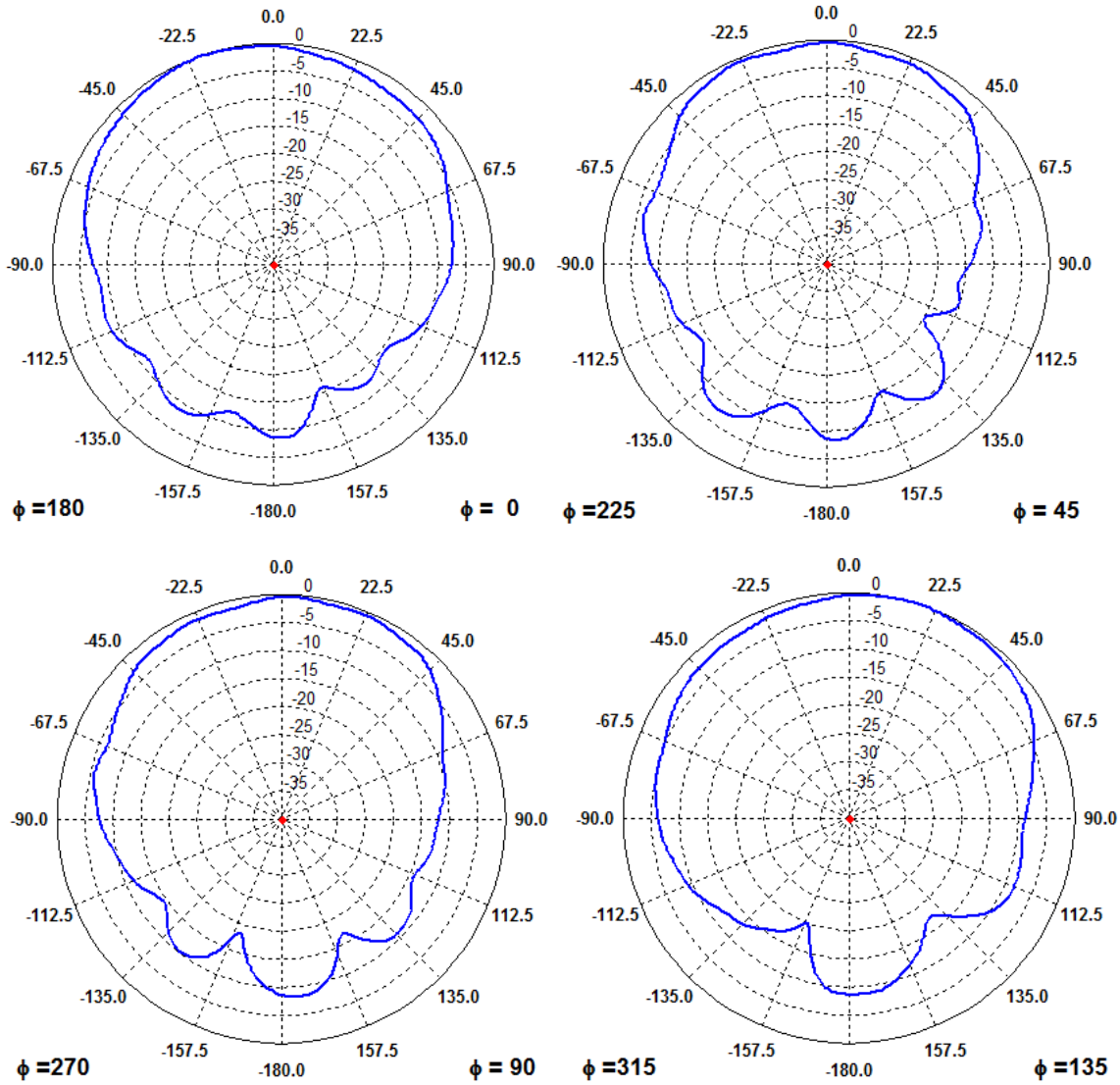

Figure 7.13. Radiation pattern cuts at 850 MHz of the antenna with resin.

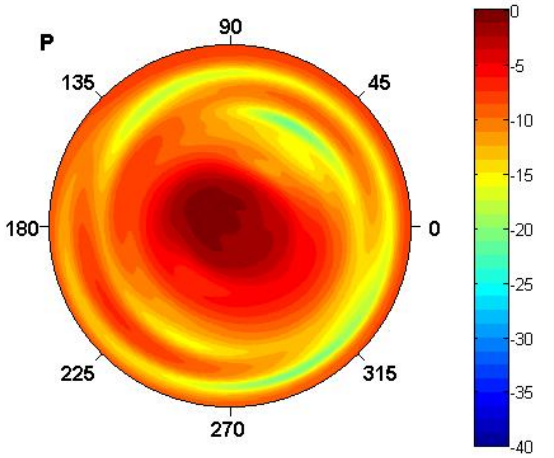

Figure 7.14. Antenna with resin front view of the radiation pattern at 850 MHz.

At 1720 MHz:

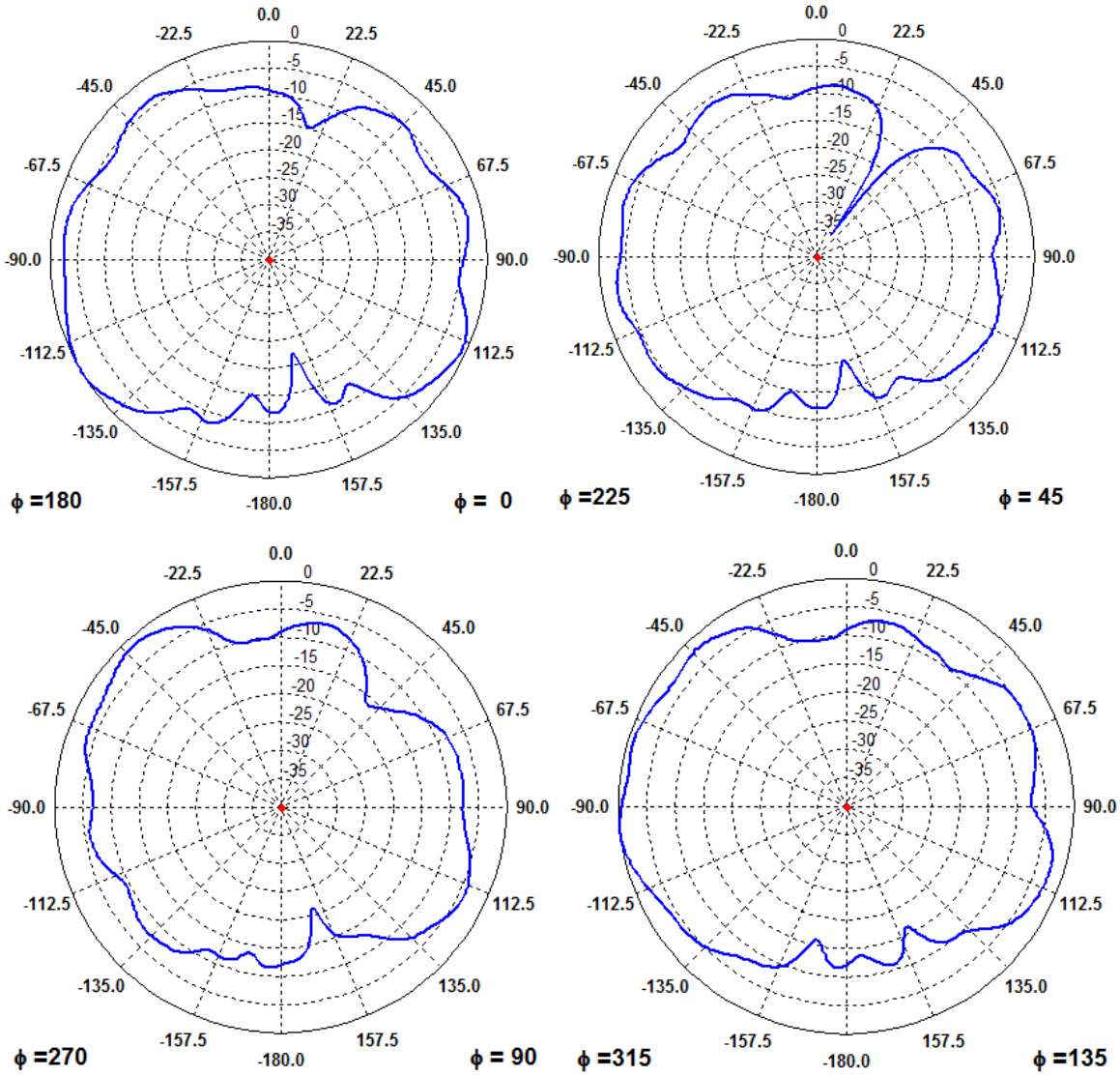

Figure 7.15. Radiation pattern cuts at 1720 MHz of the antenna with resin.

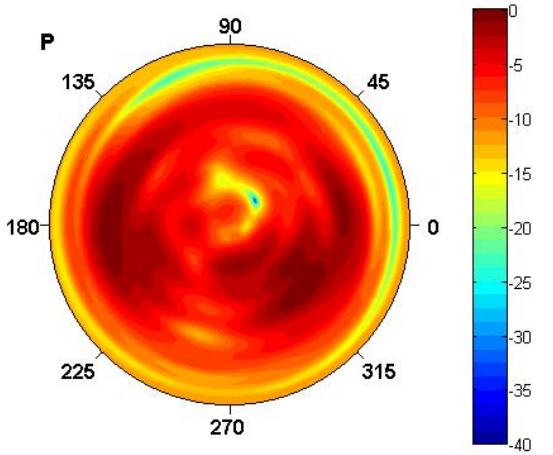

Figure 7.16. Antenna with resin front view of the radiation pattern at 1720 MHz.

At 2150 MHz:

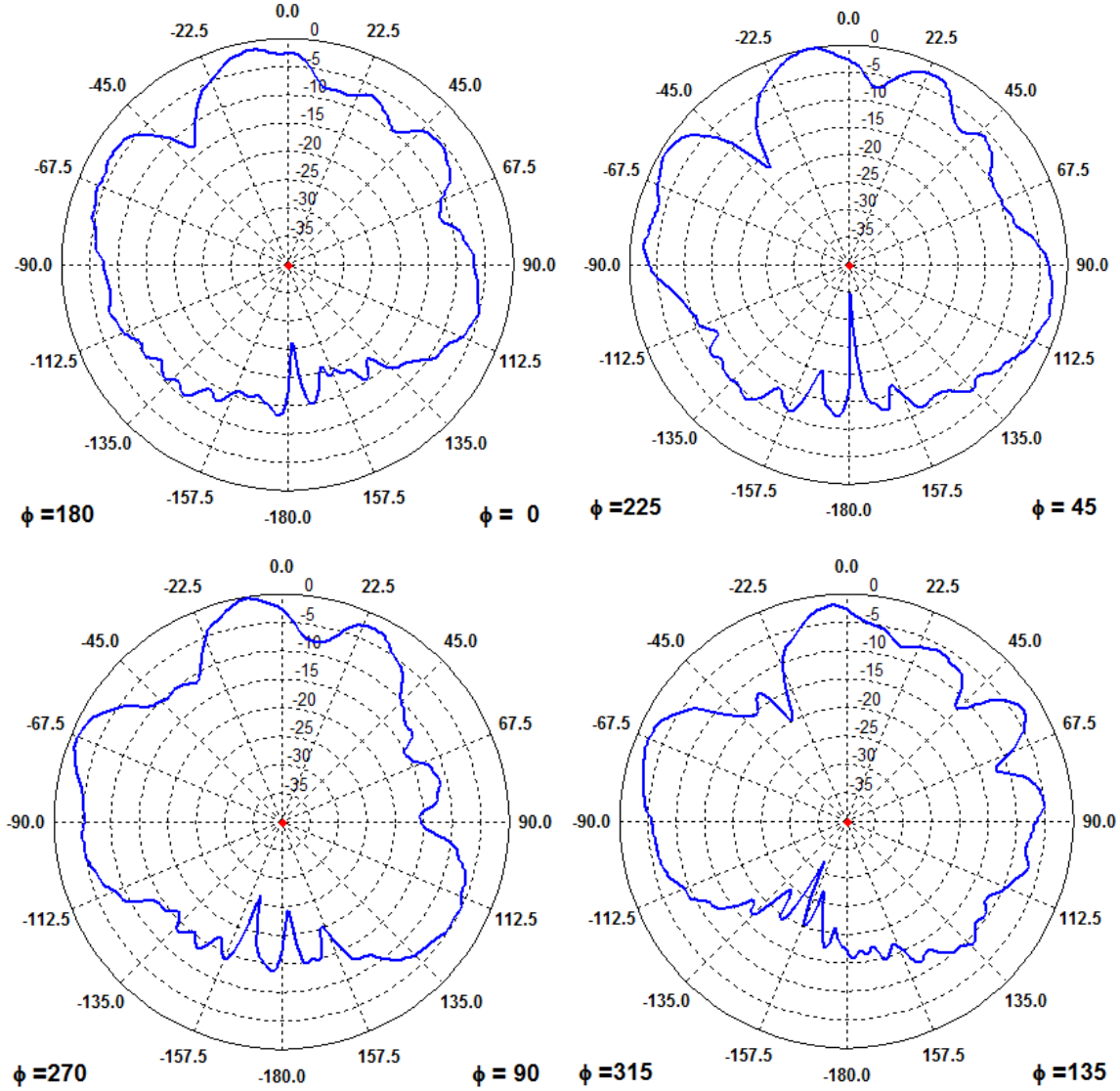

Figure 7.17. Radiation pattern cuts at 2150 MHz of the antenna with resin.

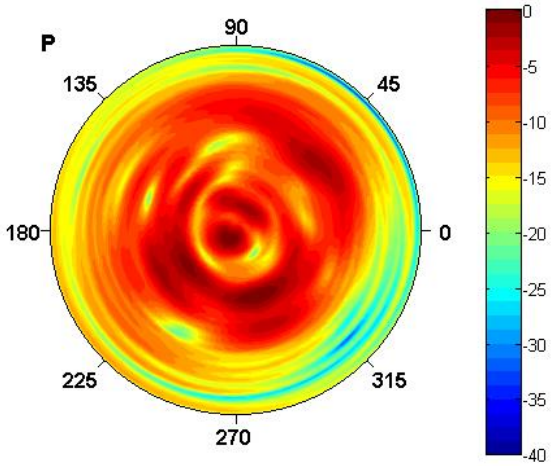

Figure 7.18. Antenna with resin front view of the radiation pattern at 2150 MHz.

Bibliography

[1] Chia-Hao Ku, Hsien-Wen Liu, Sheng-Yu Lin, “Folded Dual-Loop Antenna for GSM/DCS/PCS/UMTS Mobile Handset Applications,” IEEE Antennas and Wireless Propagation Lett., vol. 9, pp. 998-1001, Oct. 2010.

[2] International Journal of Antennas and Propagation, “IoT Antenna Design and Interaction in Complex Electromagnetic Environment,” Call for papers.
[Online] Available: http://www.hindawi.com/journals/ijap/si/905135/cfp/
[Accessed: 09 October 2016].

[3] Sheetal Kumbhar, “Antennas – squeezing the maximum value out of your spectrum”. IoTnow article, Dec 2015.
[Online] Available: http://www.iot-now.com/2015/12/08/39792-antennas-squeezing-the-maximum-value-out-of-your-spectrum/
[Accessed: 09 October 2016].

[4] S. Hayashida, T. Tanaka, H. Morishita, Y. Koyanagi, and K. Fujimoto, “Built-in folded monopole antenna for handsets,” Electron. Lett, vol. 40, no. 24, pp. 1514–1516, 2004.

[5] B. Jung, H. Rhyu, Y. J. Lee, F. J. Harackiewicz, M. J. Park, and B.Lee, “Internal folded loop antenna with tuning notches for GSM/GPS/DCS/PCS mobile handset applications,” Microw. Opt. Technol. Lett.,vol. 48, pp. 1501–1504, 2006.

[6] B.-K. Yu, B. Jung, H.-J. Lee, F. J. Harackiewicz, and B. Lee, “A folded and bent internal loop antenna for GSM/DCS/PCS operation of mobile handset applications,” Microw. Opt. Technol. Lett., vol. 48, pp.463–467, 2006.

[7] K. D. Katsibas, C. A. Balanis, P. A. Tirkas, and C. R. Birtcher, “Folded loop antenna for mobile hand-held units,” IEEE Trans.Antennas Propag., vol. 46, no. 2, pp. 260–266, Feb. 1998.

[8] C. Y. D. Sim, P.-C. Cheng, and C.-H. Lee, “Multiband loop antenna design for mobile devices,” Microw. Opt. Technol. Lett., vol. 51, pp. 2242–2248, 2009.

[9] B.-P. Su, M.-K. Sung, and G.-Y. Woon, “Broadband internal antenna by combination of a loop type antenna and a shorted monopole,” Microw. Opt. Technol. Lett., vol. 50, pp. 2810–2812, 2008.

[10] C.-H. Wu and K.-L. Wong, “Internal hybrid loop/monopole slot antenna for quad-band operation in the mobile phone,” Microw. Opt. Technol. Lett., vol. 50, pp. 795–801, 2008.

[11] Coaxial impedance calculator.
[Online] Available: https://www.eeweb.com/toolbox/coax
[Accessed: 09 October 2016].

Glossary

UMTS: Universal Mobile Telecommunication System.

CST: Computer Simulation Technology.

GSM: Global System for Mobile Communication.

DCS: Digital Cellular System.

IoT: Internet of Things.

PCB: Printed Circuit Board.

IFA: Inverted-F Antenna.

PIFA: Planar inverted-F Antenna.

FPC: Flexible printed circuit.

FR4: Flame retardant 4 material (denotes that safety of flammability is in compliance with the standard UL94V-0), FR4 is also called: Glass reinforced epoxy laminated sheets.

PCS: Personal Communication System.

CoaxL: Coaxial's length.

Coax_r: Radius of the coaxial's inner conductor (inner conductor goes from 0 to Coax_r).

Coax R: Value to determine the coaxial's dielectric thickness (dielectric goes from Coax_r to CoaxR).

CoaxR3: Value to determine the radius of the coaxial's outer conductor (outer conductor goes from CoaxR to CoaxR3).

Er: Relative permittivity.

Zo: Characteristic impedance.

g1: First gap of the proposed antenna.

g2: Second gap of the proposed antenna.

TEM: Transverse electromagnetic (electric and magnetic) waveguide mode.

Q: Quality factor.

SMA connector: SubMiniature version A connector.

VNA: Vector Network Analyser.

GPRS: General Packet Radio Service.

FBW: Fractional Bandwidth.